Volume 1 *August, 1931* *Number 2*

PHYSICS

TEMPERATURE DISTRIBUTION IN SOLID BODIES DURING HEATING OR COOLING

By J. B. Austin

Research Laboratory, United States Steel Corporation
Kearny, N. J.

(Received June 5, 1930)

Abstract

Most treatments of the problem of temperature distribution in a solid body during heating or cooling assume that the change in surface temperature is either instantaneous or linear with time. Experience shows that in many cases of practical importance the increase in surface temperature may be represented by a simple exponential function of the time. Equations for the distribution of temperature within a body when the surface is heated in accordance with this exponential relation have been derived for the following shapes: (1) rectangular parallelopiped (brick); (1a) rectangular rod; (1b) slab; (2) cylinder: (2a) cylindrical rod; (3) sphere. These equations also represent the general case of diffusion under the given boundary conditions and apply, therefore, equally well to problems such as the diffusion of one substance into another, as for instance, one metal into another.

Introduction

THE problem of the distribution of temperature within a solid body of simple geometrical shape has been discussed many times but the treatment has almost invariably been based on an assumption either of a linear rate of heating of the surface of the body or of an instantaneous change in the skin temperature from one constant value to another. The equations so derived, while quite appropriate for certain purposes, cannot, without modification, be applied to many processes of practical importance, such as the heating of cold metal masses by immersion in a hot furnace, when as is well known, the change of surface temperature cannot be regarded as following either of these assumptions.

Experimental work by the author on small steel cylinders introduced into a hot furnace, or heated from room temperature with the furnace, indicates that the surface temperature may be represented by an exponential function of the form $\theta = \theta'(1 - e^{-\beta t})$ where θ is the surface temperature at time t and θ' is the final equilibrium temperature of the surface.* The problem then, is to find equations expressing the temperature distribution within a solid when the surface is heated in accordance with this relation. The equations which have been derived as solutions of this particular problem are, of course, solutions of the general problem of diffusion in solid bodies under the aforemen-

* If the surface is cooled the exponential function is $\theta = \theta' e^{-\beta t}$.

tioned boundary conditions; they are not limited to a description of temperature distribution but may be applied to other problems of such as the diffusion of one substance into another, as for instance, one metal into another, provided always that the surface concentration varies in the manner represented by the exponential function. In these cases it is necessary only to let the symbols for temperature represent the corresponding concentration of the diffusing substance.

Since the application in which the author is chiefly interested is to the heat treatment of metals and since the important item, in this case, is the temperature distribution near the center, the solution has been given in terms of sine or cosine series since they are more convergent in this region than the probability integral, which is an alternative form of solution. The equations are, however, rigorous and perfectly general; they apply to any portion of the solid body or may be used in other ways.

For instance, anticipating a little, one of the Eqs. (41) indicates a relatively simple method for the determination of the heat diffusivity of solids. This equation gives an expression for the change of temperature at the center of a cylinder, initially at uniform temperature, when placed in a furnace at an elevated temperature. The necessary measurements can be made by means of a thermocouple attached to, or just within, the surface and another placed in a small axial hole. The latter will not appreciably disturb the equilibrium at the center since the gradient across it is zero.

The general method is that of Williamson and Adams[1] who considered the cases of linear and instantaneous change of surface temperature. Since their paper contains several typographical errors their method has been reproduced in some detail in the present paper in order that the procedure may be made clear.

Solids of the following shapes are considered: (1) Brick (rectangular parallelopiped); (1a) Rod of rectangular section, or brick with two opposite faces insulated (infinite rod); (1b) Infinite slab or thin plate; (2) Cylinder; (2a) Cylindrical rod or cylinder with insulated ends (infinite cylinder); (3) Sphere. In all cases the initial temperature is taken as uniform.*

Nomenclature

θ = difference from the initial temperature[2] at the point (x, y, z) at time t seconds from start. We shall in all cases consider the initial temperature to be 0 so that θ represents the temperature at time t seconds later.

κ = thermal diffusivity in cm^2 per second

θ' = final temperature at the surface of the metal, that is, the temperature of furnace

t = time in seconds

[1] Williamson and Adams, Phys. Rev. **14,** 99 (1919).

[2] For problems of diffusion of one substance into another substitute the appropriate concentration for temperature throughout.

* The equations as given have been derived for the case of heating of the surface. To apply them to problems of cooling $\theta=\theta'(1-e^{-\beta t})$ is replaced by $\theta e^{-\beta t}$ in the suggesged form of solution. This requires a similar substitution in the other equations and changes the sign of the summation term.

Williamson and Adams have shown that a solution of the differential equations for heat conduction or diffusion may be made up of terms which are the product of an exponential function of the time and a trigonometrical function of the coordinates, except in case (2) where Bessel's functions are required. The general form of the solution is

$$\theta = \theta'(1 - e^{-\beta t}) + \sum f(m, n, \rho) \sin \frac{m\pi x}{a} \sin \frac{n\pi y}{b} \sin \frac{p\pi z}{c}(1 - e^{-\alpha t}). \quad (1)$$

This satisfies the boundary conditions that θ must vanish for $t = 0$ and must approach θ as t increases. The exponent β must be determined experimentally but we may determine $f(m, n, p)$ and α analytically, using the general equations for heat conduction. Thus for the brick we have

$$\frac{\partial \theta}{\partial t} = k\left(\frac{\partial^2 \theta}{\partial x^2} + \frac{\partial^2 \theta}{\partial y^2} + \frac{\partial^2 \theta}{\partial z^2}\right). \quad (2)$$

By differentiating (1) we may obtain the values of the various differential coefficients in (2) and thus find values for α and $f(m, n, p)$ which satisfy the above conditions. A number of specific cases are now considered.

Case 1. Brick shape (rectangular parallelopiped). Origin of coordinates at the center of the block. Boundary conditions, $\theta = 0$, where $t = 0$, $\theta = \theta'(1 - e^{-\beta t})$ over the surface $x = \pm a$; $y = \pm b$; $z = \pm c$.

We have then:

$$\theta = \theta'(1 - e^{-\beta t}) + \sum f(m, n, p) \cos \frac{m\pi x}{2a} \cos \frac{n\pi y}{2b} \cos \frac{p\pi z}{2c}(1 - e^{-\alpha t}) \quad (3)$$

where m, n, p are integers. The equation of conduction is

$$\frac{\partial \theta}{\partial t} = k\Delta^2\theta \quad (4)$$

Following our general method we differentiate (3) and put the coefficients in (4)

$$\theta'\beta e^{-\beta t} + \sum \alpha e^{-\alpha t} f(m, n, p) \cos \frac{m\pi x}{2a} \cos \frac{n\pi y}{2b} \cos \frac{p\pi z}{2c}$$
$$\equiv -k \sum f(m, n, p)\left(\frac{m^2\pi^2}{4a^2} + \frac{n^2\pi^2}{4b^2} + \frac{p^2\pi^2}{4c^2}\right)$$
$$\cos \frac{m\pi x}{2a} \cos \frac{n\pi y}{2b} \cos \frac{p\pi z}{2c}(1 - e^{-\alpha t}) \quad (5)$$

Each side of this identity is made up of two parts, one containing $e^{-\alpha t}$ and the other not. Equating these separately yields:

$$\sum \alpha e^{-\alpha t} f(m, n, p) \cos \frac{m\pi x}{2a} \cos \frac{n\pi y}{2b} \cos \frac{p\pi z}{2c}$$

$$= - k \sum f(m, n, p)\left(\frac{m^2\pi^2}{4a^2} + \frac{n^2\pi^2}{4b^2} + \frac{p^2\pi^2}{4c^2}\right) \cos\frac{n\pi x}{2a} \cos\frac{n\pi y}{2b} \cos\frac{p\pi z}{2c}\, e^{-\alpha t} \quad (6)$$

and

$$\theta'\beta e^{-\beta t} = - k \sum f(m, n, p)\left(\frac{m^2\pi^2}{4a^2} + \frac{n^2\pi^2}{4b^2} + \frac{p^2\pi^2}{4c^2}\right) \cos\frac{m\pi x}{2a} \cos\frac{n\pi y}{2b} \cos\frac{p\pi z}{2c} \quad (7)$$

From (6) we obtain at once

$$\alpha = - k\left(\frac{m^2\pi^2}{4a^2} + \frac{n^2\pi^2}{4b^2} + \frac{p^2\pi^2}{4c^2}\right) \quad (8)$$

To evaluate (7) we need the series

$$\frac{\pi}{4} = \cos\frac{\pi x}{2a} - \frac{1}{3}\cos\frac{3\pi x}{2a} + \frac{1}{5}\cos\frac{5\pi x}{2a} + \cdots \quad (9)$$

which holds between $x = +a$ and $x = -a$.

Multiplying together 3 such series yields

$$\frac{\pi^3}{64} = \sum(-1)^{m+n+p+1} \frac{\cos[(2m-1)\pi x/2a]\cos[(2n-1)\pi y/2b]\cos[(2p-1)\pi z/2c]}{(2m-1)(2n-1)(2p-1)} \quad (10)$$

where m, n, p are all positive integers.

Eq. (7) will reduce to this if $f(m, n, p)$ be put equal to

$$\frac{64\theta'\beta e^{-\beta t}}{k\pi^3} \cdot \frac{(-1)^{m+n+p+1}}{(2m-1)(2n-1)(2p-1)\left\{\frac{(2m-1)^2\pi^2}{4a^2} + \frac{(2n-1)^2\pi^2}{4b^2} + \frac{(2p-1)^2\pi^2}{4c^2}\right\}} \quad (11)$$

Substitution of these values in (3) gives:

$$\theta = \theta'(1 - e^{-\beta t}) - \frac{64\theta'\beta e^{-\beta t}}{k\pi^3} \sum_{m,n,p=1}^{p,n,m=\infty} (-1)^{m+n+p+1} \frac{\cos[(2m-1)\pi x/2a]\cos[(2n-1)\pi y/2b]\cos[(2p-1)\pi z/2c]}{(2m-1)(2n-1)(2p-1)\left\{\frac{(2m-1)^2\pi^2}{4a^2} + \frac{(2n-1)^2\pi^2}{4b^2} + \frac{(2p-1)^2\pi^2}{4c^2}\right\}} \left(1 - \exp - k\left\{\frac{(2m-1)^2\pi^2}{4a^2} + \frac{(2n-1)^2\pi^2}{4b^2} + \frac{(2p-1)^2\pi^2}{4c^2}\right\}t\right) \quad (12)$$

By substituting Q_m, Q_n, Q_p for $(2m-1)\pi/2$, $(2n-1)\pi/2$, $(2p-1)\pi/2$ respectively we get

$$\theta = \theta'(1 - e^{-\beta t}) - \frac{8\theta'\beta e^{-\beta t}}{k} \sum_{m,n,p=1}^{p,n,m=\infty} (-1)^{m+n+p+1} \frac{\cos Q_n x/a \cos Q_n y/b \cos Q_p 3/c}{Q_m, Q_n, Q_p(Q_m^2/a^2 + Q_n^2/b^2 + Q_p^2/c^2)}(1 - e^{-k[Q_m^2/a^2+Q_n^2/b^2+Q_p^2/c^2]t}) \quad (13)$$

Case 1 (a). Rectangular rod. This case may be deduced directly from (13) by assuming that c is large compared to a and b.

$$\theta = \theta'(1 - e^{-\beta t}) - \frac{4\theta'\beta e^{-\beta t}}{k} \sum_{m,n=1}^{m,n=\infty} (-1)^{m+n+1} \frac{\cos (Q_m x/a) \cos (Q_n y/b)}{Q_m, Q_n(Q_m^2/a^2 + Q_n^2/b^2)}(1 - e^{-k[Q_m^2/a^2+Q_n^2/b^2]t}) \quad (14)$$

Case 1 (b). Infinite slab. This case also may be deduced from (13) by assuming both b and c as large compared to a.

$$\theta = \theta'(1 - e^{-\beta t}) - \frac{2\theta'\beta e^{-\beta t}}{k} \sum_{m=1}^{m=\infty}(-1)^{m+1}\frac{\cos (Q_m x/a)}{Q_m^3/a^2}(1 - e^{-k(Q_m^2/a^2)t}) \quad (15)$$

Case 2. Cylinder. Radius $= a$, length $= 2b$. Origin of coordinates at center. In this case the computation is simplified if we introduce Bessel's functions in place of the cosine terms in the radial direction. Only the following properties of Bessel's functions are required in the derivation.

$$J_0(x) = 1 - \frac{x^2}{2^2} + \frac{x^4}{2^2 \times 4^2} - \frac{x^6}{2^2 \times 4^2 \times 6^2} + \cdots \quad (16)$$

$$\frac{dJ_0(x)}{dx} = -J_1(x) \quad (17)$$

$$\frac{dJ_1(x)}{dx} = J_0(x) - \frac{1}{x}J_1(x) \quad (18)$$

$$\sum_{m=1}^{m=\infty} \frac{2}{R_n J_1(R_n)} J_0\left(R_n \frac{x}{a}\right) = 1. \quad (19)$$

The suggested form of solution is:

$$\theta = \theta'(1 - e^{-\beta t}) + \sum f(m, R_n) J_0\left(R_n \frac{x}{a}\right) \cos \frac{m\pi z}{2b}(1 - e^{-\alpha t}). \quad (20)$$

The equation of conduction is

$$\frac{\partial \theta}{\partial t} = k\left(\frac{\partial^2 \theta}{\partial x^2} + \frac{1}{x}\frac{\partial \theta}{\partial x} + \frac{\partial^2 \theta}{\partial z^2}\right). \quad (21)$$

By reasoning similar to that used in considering the brick and by using (9) and (19) we obtain

$$\theta = \theta'(1 - e^{-\beta t}) - \frac{8\theta'\beta e^{-\beta t}}{\pi k} \sum_{m,n=1}^{n,m=\infty} \frac{(-1)^{m+1}}{(2m-1)} \frac{J_0(R_n(x/a))\cos((2m-1)\pi z/2b))}{\left(\frac{R_n^2}{a^2} + \frac{(2m-1)^2\pi^2}{4b^2}\right) R_n J_1(R_n)} \left(1 - \exp - k\left\{\frac{R_n^2}{a^2} + \frac{(2m-1)^2\pi^2}{4b^2}\right\} t\right) \quad (22)$$

Case 2 (a). Cylindrical rod. When b becomes large compared to a we get

$$\theta = \theta'(1 - e^{-\beta t}) - \frac{2\theta'\beta e^{-\beta t} a^2}{k} \sum_{n=1}^{n=\infty} \frac{J_0(R_n(x/a))}{R_n^3 J_1(R_n)} \left(1 - exp - k\frac{R_n^2}{a^2} t\right). \quad (23)$$

Case 3. Sphere of radius a, origin at center. The suggested form of solution is

$$\theta = \theta'(1 - e^{-\beta t}) + \sum_{m=1}^{m=\infty} f(m) \frac{1}{x} \sin \frac{m\pi x}{a} (1 - e^{-\alpha t}). \quad (24)$$

The equation of conduction is:

$$\frac{\partial(x\theta)}{\partial t} = k \frac{\partial^2(x\theta)}{\partial x^2}. \quad (25)$$

Following our usual procedure we get

$$x\theta'\beta e^{-\beta t} + \sum \alpha e^{-\alpha t} f(m) \sin \frac{m\pi x}{a} \equiv - k \sum f(m) \frac{m^2\pi^2}{a^2} \sin \frac{m\pi x}{a} (1 - e^{-\alpha t}) \quad (26)$$

whence

$$\alpha = - k \frac{m^2\pi^2}{a^2} \quad (27)$$

and since

$$\sum \frac{x}{\sin \frac{m\pi x}{a}} (-1)^{m+1} = \frac{2a}{m\pi} \quad (28)$$

$$\therefore f(m) = \frac{\theta'\beta e^{-\beta t}}{k} \cdot \frac{2a}{m\pi} \cdot \frac{a^2}{m^2\pi^2}. \quad (29)$$

Hence

$$\theta = \theta'(1 - e^{-\beta t}) - \frac{2a^2\theta'\beta e^{-\beta t}}{k} \sum_{m=1}^{m=\infty} \frac{(-1)^{m+1}}{m^3\pi^3} \frac{a}{x} \sin \frac{m\pi x}{a} (1 - e^{-k(m^2\pi^2/a^2)t}). \quad (30)$$

In many cases we are interested in the temperature at the center of the body ($x=0, y=0, z=0$). In this case all the cosine terms and J_0 terms become unity and we obtain

Brick

$$\theta = \theta'(1 - e^{-\beta t}) - \frac{8\theta'\beta e^{-\beta t}}{k} \sum_{m,n,p=1}^{p,n,m=\infty} (-1)^{m+n+p+1} \frac{1}{Q_m, Q_n, Q_p, \left(\frac{Q_m^2}{a^2} + \frac{Q_n^2}{b^2} + \frac{Q_p^2}{c^2}\right)} \left(1 - \exp - k\left\{\frac{Q_m^2}{a^2} + \frac{Q_n^2}{b^2} + \frac{Q_p^2}{c^2}\right\} t\right). \quad (31)$$

Rectangular rod

$$\theta = \theta'(1 - e^{-\beta t}) - \frac{4\theta'\beta e^{-\beta t}}{k} \sum_{m,n=1}^{n,m=\infty} (-1)^{m+n+1} \frac{1}{Q_m, Q_n, \left(\frac{Q_m^2}{a^2} + \frac{Q_n^2}{b^2}\right)} \left(1 - \exp - k\left\{\frac{Q_m^2}{a^2} + \frac{Q_n^2}{b^2}\right\} t\right). \quad (32)$$

Infinite slab

$$\theta = \theta'(1 - e^{-\beta t}) - \frac{2\theta'\beta e^{-\beta t}}{k} \sum_{m=1}^{m=\infty} (-1)^{m+1} \frac{a^2}{Q_m^3} \left(1 - \exp - k\frac{Q_m^2}{a^2} t\right). \quad (33)$$

Cylinder

$$\theta = \theta'(1 - e^{-\beta t}) - \frac{8\theta'\beta e^{-\beta t}}{\pi k} \sum_{m,n=1}^{n,m=\infty} (-1)^{m+1} \frac{1}{(2m-1)\left(\frac{R_n^2}{a^2} + \frac{m^2\pi^2}{4b^2}\right) R_n J_1(R_n)} \left(1 - \exp - k\left\{\frac{R_n^2}{a^2} + \frac{m^2\pi^2}{b^2}\right\} t\right). \quad (34)$$

Cylindrical rod

$$\theta = \theta'(1 - e^{-\beta t}) - \frac{2a^2\theta'\beta e^{-\beta t}}{k} \sum_{m=1}^{m=\infty} \frac{1}{R_n^3 J_1(R_n)} \left(1 - \exp - k\frac{R_n^2}{a^2} t\right). \quad (35)$$

Sphere

$$\theta = \theta'(1 - e^{-\beta t}) - \frac{2a^2\theta'\beta e^{-\beta t}}{k} \sum_{m=1}^{m=\infty} \frac{(-1)}{m^3\pi^3} \left(1 - \exp - k\frac{m^2\pi^2}{a^2} t\right). \quad (36)$$

A still further simplification may be introduced. As the time t increases the exponential terms approach zero and the terms involving the product of $e^{-\alpha t}$ and $e^{-\beta t}$ in the final equations are small compared to the others. This simplification may be applied to any of the equations but the ones for the center of the bodies are given below:

Brick

$$\theta = \theta'(1 - e^{-\beta t}) - \frac{8\theta'\beta e^{-\beta t}}{k} \sum_{m,n\,p=1}^{p,n,m=\infty} \frac{(-1)^{m+n+p+1}}{Q_m, Q_n, Q_p, \left(\frac{Q_m^2}{a^2} + \frac{Q_n^2}{b^2} + \frac{Q_p^2}{c^2}\right)}. \quad (37)$$

Rectangular rod

$$\theta = \theta'(1 - e^{-\beta t}) - \frac{4\theta'\beta e^{-\beta t}}{k} \sum_{m,n,=1}^{n,m,=\infty} \frac{(-1)^{m+n+1}}{Q_m, Q_n, \left(\frac{Q_m^2}{a^2} + \frac{Q_n^2}{b^2}\right)}. \quad (38)$$

Infinite slab

$$\theta = \theta'(1 - e^{-\beta t}) - \frac{2a^2\theta'\beta e^{-\beta t}}{k} \sum_{m=1}^{m=\infty} \frac{(-1)^{m+1}}{Q_m^3}. \quad (39)$$

Cylinder

$$\theta = \theta'(1 - e^{-\beta t}) - \frac{8\theta'\beta e^{-\beta t}}{\pi k} \sum_{m=1,n=1}^{n=\infty,\,m=\infty} \frac{(-1)^{m+1}}{(2m-1)\left(\frac{R_n^2}{a^2} + \frac{m^2\pi^2}{4b^2}\right) R_n J_1(R_n)}. \quad (40)$$

Cylindrical rod

$$\theta = \theta'(1 - e^{-\beta t}) - \frac{2\theta'\beta e^{-\beta t}}{k} \sum_{n=1}^{n=\infty} \frac{1}{R_n^3 J_1(R_n)}. \quad (41)$$

Sphere

$$\theta = \theta'(1 - e^{-\beta t}) - \frac{2\theta'\beta e^{-\beta t}}{k} \sum_{m=1}^{m=\infty} \frac{(-1)^{m+1}}{m^3\pi^3}. \quad (42)$$

Eqs. (37) to (42) have the advantage that they make it possible to express k explicitly in terms of the other variables. In all the relations previously discussed this is not easily accomplished, if indeed it is possible at all, and if k is to be determined resort must be had to some method of approximation. The foregoing equations and the ones to follow are thus especially adapted to the measurement of the diffusivity.

It will also be observed that in the equations for the so-called "unidimensional solids," i.e., solids in which heat flows in one dimension only as for instance in the slab (39), cylindrical rod (41) and sphere (42), the term under the summation sign does not involve any of the variables in the problem; hence, remembering that $Q_m = (2m-1)\pi/2$ we may replace the summation term by a numerical value. This operation leads to the following equations which have been rearranged to show their similarity of form:

Infinite slab

$$\theta = \theta'(1 - e^{-\beta t}) - \frac{2a^2\theta'\beta e^{-\beta t}}{k}(0.2308). \tag{43}$$

Cylindrical rod

$$\theta = \theta'(1 - e^{-\beta t}) - \frac{2a^2\theta'\beta e^{-\beta t}}{k}(0.1247). \tag{44}$$

Sphere

$$\theta = \theta'(1 - e^{-\beta t}) - \frac{2a^2\theta'\beta e^{-\beta t}}{k}(0.0291). \tag{45}$$

The equations for the cube and for the rod of square cross section, can, obviously, be made to assume the same form.

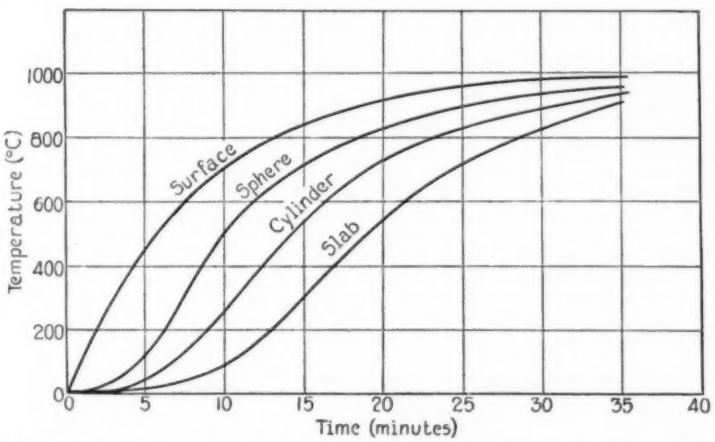

Fig. 1. Temperature distribution in solid bodies during heating or cooling.

The distribution of temperature within the body described by these equations is quite similar to that obtained with linear heating of the surface; such a distribution is well known and has been shown by many others, so that no discussion need be given here. It is interesting, however, to investigate the variation with time of the temperature at the center of bodies of simple geometrical shape under the heating conditions postulated. This variation has been calculated for the unidimensional solids and is shown in Fig. 1. The following values have been assumed in making the calculations $\theta' = 1000°C$. $\beta = 2 \times 10^{-3}$, $k = 0.010$ cm^2/sec., $a = 7.5$ cm. The values of β and k are rounded values based on on actual experience of the author in dealing with steel cylinders.

It will be seen at once, that for a given thickness, or radius, temperature equalization is attained most rapidly in a sphere and least rapidly in a slab, which is the order observed with the common boundary conditions. Other general relations of the curves of Fig. 1 are obvious and need no further discussion. These remarks apply, *mutatis mutandis*, to other cases of diffusion under the same boundary conditions.

SOME THERMIONIC PROPERTIES OF BARIUM FILMS ADSORBED ON TUNGSTEN

By Herbert Nelson

Development Laboratories RCA Radiotron Company, Inc., Harrison, N. J.

(Received April 2, 1931)

Abstract

An investigation has been made of some thermionic properties of a barium film adsorbed on tungsten for various values of θ, the fraction of the surface covered with barium. The experimental tube was so constructed that the measurements could be made on a small area of the filament in order that errors due to lead losses, non-uniformities, and voltage drop along the filament might be minimized. An electrometer vacuum tube was used to measure the electron currents. The experimental results obtained by Eglin were confirmed, i.e. the thermionic activity of the composite surface was found to increase with θ until an optimum value was reached after which further deposit of barium caused the activity to decrease. As a result of prolonged deposition, a steady value of the activity was reached which did not change appreciably or regularly with further deposition. The change in C.D.P. was found to be directly proportional to the change in T_θ, the absolute temperature of the filament required to give an arbitrarily fixed value of electron emission. It is significant that the factor of proportionality for all values of the activity higher than the steady value reached after prolonged deposition was found to be different than that obtained for the values which were lower. The distribution of velocities of the emitted electrons was found to be Maxwellian for all values of θ. The construction of the experimental tube was found to be unsuitable for studying the effect of field intensity on the activity. Thus the results obtained pertaining to this effect are of little significance.

IT IS a well-known fact that the theories of thermionic emission as derived for clean metal surfaces do not fit experimental facts obtained for composite surfaces. The coefficient A of the thermionic emission equation $I = AT^2\epsilon^{-\phi e/kT}$ which theoretically is a universal constant for pure metals varies widely for composite surfaces. The Schottky theory accounts satisfactorily for the effect of field strength on the emission from clean metal surfaces. It fails, however, to account for the effects observed in the case of composite surfaces. Experimental evidence indicates that ϕ for clean metals is independent of temperature. The results obtained for composite surfaces, on the other hand, have led J. A. Becker,[1] Schottky,[2] and others to the belief that the work function of a composite surface is dependent upon the temperature.

Theories have been advanced by Langmuir,[3] Becker,[4] and others to account for the thermionic behavior of composite surfaces. Though these theo-

[1] J. A. Becker, Phys. Rev. **34,** 1323 (1929).

[2] Schottky, Rothe and Simon, vol. 13, of Wien Harms, "Handbuch der Experimentalphysic."

[3] Langmuir, Gen. Elec. Rev. **23,** 504 (1920).

[4] Becker and Mueller, Phys. Rev. **31,** 431 (1928).

ries may be qualitatively correct they are apparently not complete in so far as they fail to account for the effect of field strength on the emission at low accelerating potentials.[5]

In view of the above, an investigation which might throw more light on the thermionics of composite surfaces appeared to be in order. In this investigation, therefore, the following thermionic phenomena were studied: I. The change in thermionic activity and contact potential difference (C.D.P.) caused by depositing barium on tungsten. II. The relation between change in activity and change in C.D.P. III. The effect of field strength on the activity and on the C.D.P. IV. The distribution of velocities of the emitted electrons for various values of θ, the fraction of the surface covered with barium.

Experimental Arrangement

A diagram of the apparatus is shown in Fig. 1. The experimental tube contains the anode A, the collector C, the tungsten ribbon filament W, and the barium oxide coated filaments O_1 and O_2. The anode consists of two parallel plates electrically connected. The filaments are kept taut by means of tungsten springs. The oxide coated filaments are mounted perpendicularly with respect to the tungsten filament in such a manner that the "beams" of

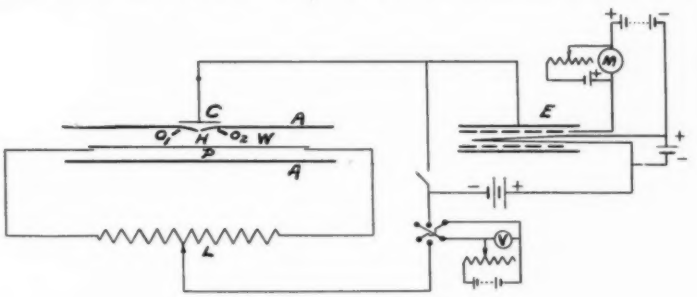

Fig. 1. Diagram of apparatus.

material evaporated from the barium oxide coating are "focused" on the point P of the tungsten ribbon directly opposite the aperture H in the anode. (In this experiment the filaments were glowed under such conditions that the material evaporated could be assumed to be barium.)[1] The plate C serves as a collector for the electron beam through the aperture.

The anode plates were 7.5 cm long, 3.0 cm wide, and were spaced 1.2 cm apart. The average thickness and width of the tungsten filament W were 0.0025 cm and 0.0497 cm respectively. It was 7.0 cm long. The aperture H was 0.1 cm in diameter. The perpendicular distance between the aperture H and the tungsten ribbon was 0.6 cm.

Precautions were taken to insure a high leakage resistance between the collector and the other electrodes of the tube. The electron current to C, I_c, was measured by means of the electrometer tube arrangement E.[6] The electrometer tube and the experimental tube were enclosed in a brass tube closed

[5] Compton and Langmuir, Reviews of Modern Physics **2**, 150 (1930).

[6] H. Nelson, The Rev. of Scientific Instr. **1**, 281 (1930).

at the ends by bakelite disks through which the leads were brought out. The brass tube served as an electrostatic shield and as a means of keeping the tubes in dry air to prevent electrical leakage over the glass.

The experimental tubes used in the investigation were thoroughly exhausted before being sealed off. The tubes were baked during exhaust and the metal parts were degassed. After the tubes had been sealed off from the pumping system, the vacuum was further improved by the glowing of auxiliary thoriated tungsten filaments. The excellent reproducibility of experimental results indicated that good vacuum conditions were obtained.

Method

A relative measure of the activity of the tungsten surface for various degrees of covering with barium was obtained by determining the absolute temperature T_θ of the filament necessary to cause an electron current of 1.9×10^{-12} amperes to flow to the collector C, the anode and the collector being fixed at a positive potential of six volts with respect to the point P on the tungsten ribbon.

From the Richardson equation of thermionic emission

$$I = AT^2\epsilon^{-\phi\epsilon/kT}$$

it follows that the relation between T_θ and the commonly accepted measure of thermionic activity, ϕ, may be expressed as follows:

$$\phi_\theta = T_\theta/11600[\ln a + 2\ln T_\theta - \ln(1.9\times10^{-12}) + \ln A_\theta]$$

where ϕ_θ and A_θ are the values of ϕ and A, expressed in volts and amp./cm^2 deg^2. respectively, when the fraction of the surface covered is equal to θ and where a is the effective emitting area in cm^2. The value 11,600 deg./volt has been substituted for the ratio e/k.

Though the value of a may be obtained experimentally by measuring the electron current to the collector at a known temperature of the clean tungsten ribbon, it is apparent that the value of ϕ_θ may be determined through measurements of T_θ only when A_θ is known.

The temperature at the point P of the tungsten filament corresponding to a definite filament current was determined from calculations based upon a knowledge of the dimensions of the ribbon and data published by Langmuir and Jones.[7] End loss corrections were calculated in accodrance with the best published data.[8] An experimental check on the calculated results was obtained through pyrometer measurements. In Fig. 2 the temperature of point P of the tungsten ribbon is plotted as a function of the filament current. The points marked by circles are the calculated values; those marked by triangles are the ones obtained through pyrometer measurements. The points marked by crosses were calculated from Maxwellian distribution curves.

The contact potential difference, V_c, between the point P on the tungsten ribbon and the collector C was determined from Maxwellian distribution

[7] H. A. Jones and I. Langmuir, Gen. Elec. Rev. **30**, 310, 354, 408 (1927).
[8] I. Langmuir, S. MacLane and K. B. Blodgett, Phys. Rev. **35**, 478 (1930).

curves. The data for these curves were obtained by measuring I_e, the electron current to the collector C, for low positive and negative potentials of C with respect to the point P. (The contact at the point L [See Fig. 1] had been so adjusted that it was at the same potential as the point P on the tungsten ribbon for all values of the filament current.) The anode was maintained at a constant positive potential of six volts with respect to the point P during the

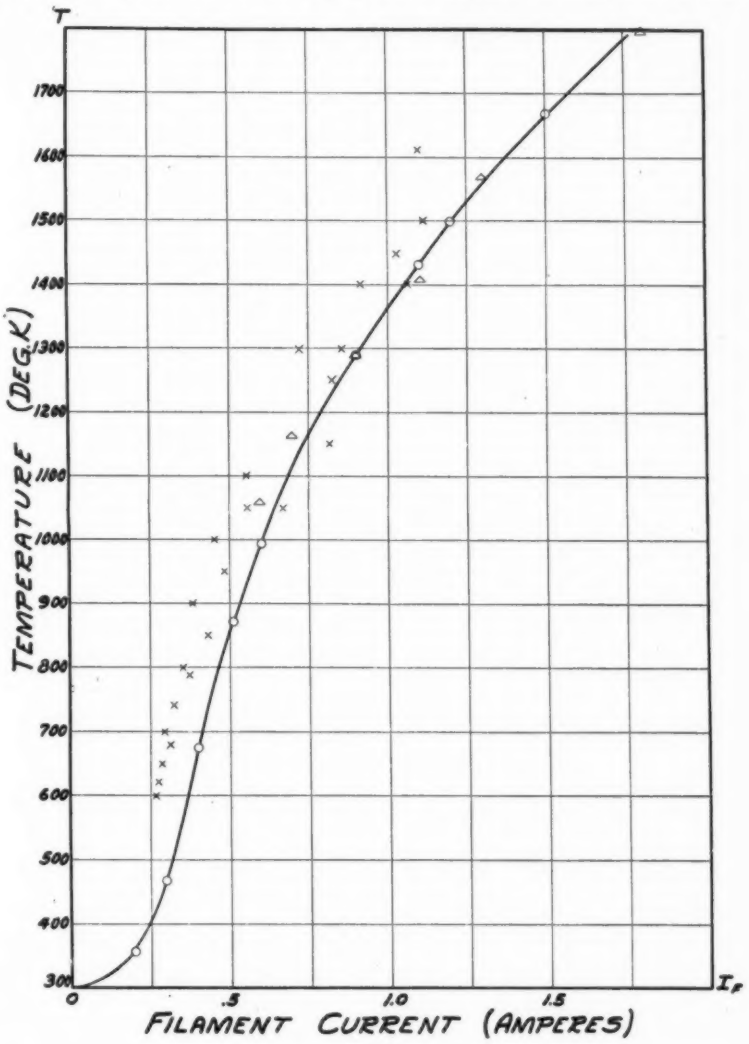

Fig. 2.

measurements. In Fig. 6 are shown Maxwellian distribution curves typical of the ones obtained in the experiment. The value of V at the point O was taken as the C.D.P. Theoretically the point O defines the state at which the point P and the collector are at the same potential.[9] Thus at this point the externally applied potential is equal but opposite to the C.D.P.

[9] N. B. Reynolds, Phys. Rev. **35**, 163 (1930).

To determine the relation between V_c and T_θ, their values were determined simultaneously for various values of θ.

The effect of field intensity on the C.D.P. and on the activity of the emitting surface was investigated by obtaining Maxwellian distribution curves for various anode potentials and by studying I_c, the electron current to the collector, as a function of the anode potential V_a at a constant potential of the collector.

Experimental Results

I. The thermionic activity and the C.D.P. as functions of θ.

The graph in Fig. 3 shows how V_c varies with the time of evaporation. The temperature of the oxide coated filaments during the evaporation was estimated at 1200°K.

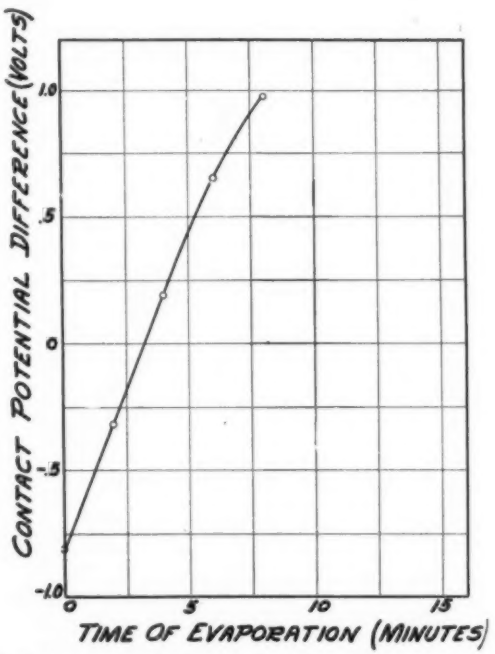

Fig. 3. Change in C.D.P. between collector and cathode with time of evaporation of barium.

It is evident that there can exist a definite relation between the value of θ and the time of evaporation only when no migration[10] of barium occurs on the tungsten surface. This condition appears to be fulfilled for $\theta < 1/2$. For larger values of θ, migration seems to occur at the temperature at which the measurements are made. For this reason no attempts were made to obtain a quantitative relation between V_c and T_θ for values of $\theta > 1/2$. On the other hand a qualitative relation between V_c and T_θ for the larger values of θ could be obtained on the obvious assumption that θ increases with the time of evaporation. Thus it was found that V_c increased and T_θ decreased with θ until a

[10] Becker, "The Life History of Adsorbed Atoms and Ions" Proc. Am. Electrochem. Soc. 55, 153 (1929).

maximum V_c and a minimum T_θ were reached after which further evaporation caused V_c to decrease and T_θ to increase. This is in agreement with the results obtained by Eglin[11] who found maximum activity of barium on tungsten for a value of θ he assumed to be equal to one, and lower activities for $\theta > 1$.

After the activity had passed the maximum, it reached a lower and practically constant value which did not vary appreciably or regularly with further evaporation. This value of the activity was assumed to be that characteristic of barium metal. As the "thick" film of barium was removed from the tungsten ribbon by flashing it, the activity at first increased and then, after having reached a maximum, decreased as more and more barium was being removed until finally the state of clean tungsten was reached.

The C.D.P. was always found to vary regularly with the activity and whenever the activity passed through a maximum the C.D.P. also passed through a maximum.

Three separate determinations of the value of T_θ for a "thick" film of barium was made. The values obtained for the first, second, and third run were respectively 465°K, 465°K, and 460°K. The corresponding values obtained for V_c were 2.0, 2.05, and 2.1 volts. For the maximum activity observed

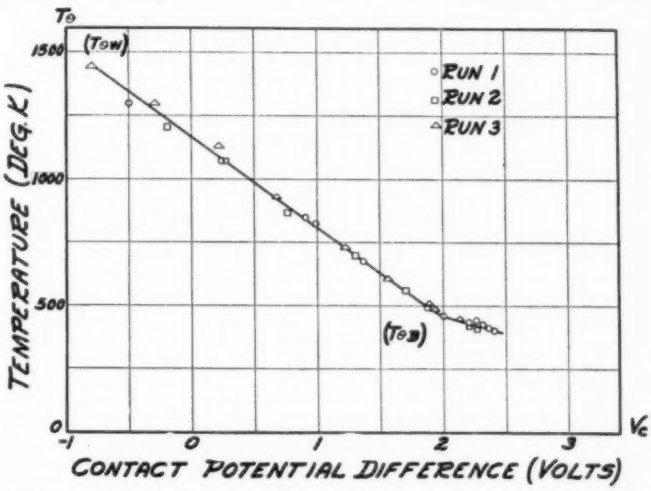

Fig. 4. T is plotted as a function of the C.D.P. between collector and cat hode.

the values for T_θ and V_c were found to be 410°K and 2.39 volts respectively. The values of T_θ and V_c for clean tungsten were 1450°K and -0.81 volts.

II. Relation between V_c and T_θ.

The curve in Fig. 4 shows the relation between V_c and T_θ as obtained experimentally. It was plotted from data obtained in three separate runs. The curve shows a straight line relation between V_c and T_θ between $T_{\theta W}$ and $T_{\theta B}$. $T_{\theta W}$ is the value of T_θ observed for clean tungsten and $T_{\theta B}$ is the lowest value observed for a "thick" layer of barium. At the point corresponding to $T_{\theta B}$ there is a break in the curve, T_θ varying less rapidly with V_c for the values that are higher than for those which are lower than $T_{\theta B}$. In Fig. 5 the region

[11] Eglin, Phys. Rev. **31**, 1127 (1928).

of the break has been plotted on an enlarged scale. The points marked by circles were obtained in the process of depositing barium while those marked by triangles were obtained in the process of removing barium.

In the present experiment V_c was measured to an accuracy of about 0.05 volts. It is more difficult to estimate the accuracy of the temperature calculations, especially in the lower range where corrections due to end losses must be made. In this region it is also possible that an appreciable error has been introduced in the temperature calculations due to the failure of taking into consideration the effect of the barium film on the radiation coefficient of tungsten.

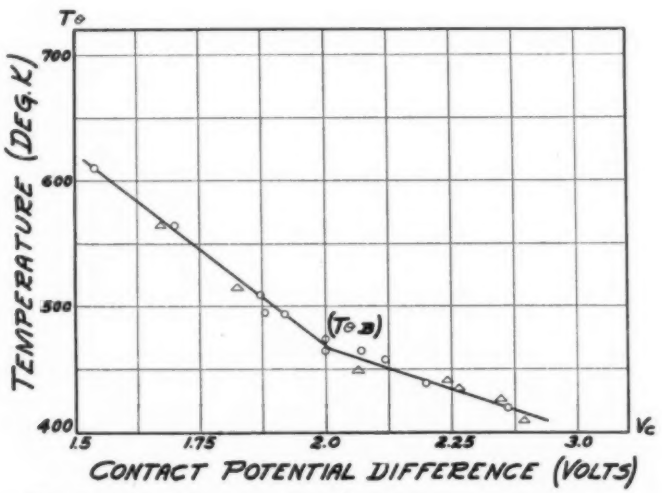

Fig. 5. The region of the break of the curve shown in Fig. 4.

In view of the above it follows that while the curve in Fig. 4 cannot be considered as giving the exact relation between V_c and T_θ, especially at low values of T_θ (high values of the activity), the observed linearity in the relationship between V_c and T_θ, however, is sufficiently definite, and the break observed at $T_{\theta B}$, sufficiently sharp to make the curve significant.

It appears, on the other hand, that a more accurate investigation of the relation between V_c and T_θ simultaneously with determinations of the work function, ϕ, and the A constant of the thermionic emission equation for various values of θ, is desirable before attempts are made to interpret theoretically the results obtained. Such an investigation is now in progress in these laboratories.

III. Velocity distribution determinations.

The velocity distribution curves in Fig. 6 were obtained by plotting the logarithm of the current to the collector as a function of the potential difference between the collector and the point P on the tungsten filament. Curve A is for a clean tungsten surface at temperature of 1423°K. Curve B was obtained for a barium on tungsten surface at a temperature of 700°K.

On the assumption that the distribution of velocities of the emitted electrons is a Maxwellian one, Richardson shows that for parallel electrodes the

relation between retarding potentials and electron current may be expressed by the equation[12]

$$i = i_0 \epsilon^{-V_1 e/kT}$$

where i_0 is the value of i at $V_1 = 0$. V_1 is the retarding potential, e is the electronic charge, k is the Boltzmann constant, and T is the temperature of the electron source.

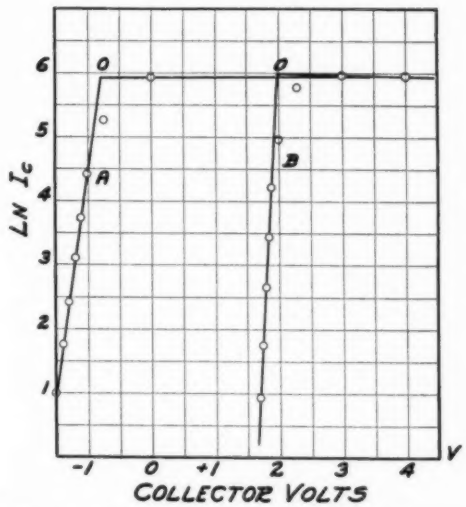

Fig. 6. Typical Maxwellian distribution curves.

The above equation may be written

$$\ln i = -V_1 e/kT + \ln i_0.$$

Thus if $\ln i$ is plotted as a function of V_1, the slope of the resulting straight line should be equal to e/kT. Since e and k are known constants it is evident that the temperature of the electron source may be determined from the slope of the velocity distribution curve.

In Fig. 2 the temperatures corresponding to the points marked by crosses were calculated from Maxwellian distribution curves. These temperatures are on the average considerably higher than the true temperature of the filament. Such a disparity between true temperature and temperature as calculated from Maxwellian distribution curves has been a common observation in previous investigations of composite surfaces.[13]

IV. Effect of field intensity on activity.

Curves such as are shown in Fig. 7 were obtained in studying the effect of field intensity on the thermionic activity for various values of θ. The data for these curves were obtained by measuring the electron current I_c to the collector for different values of the anode potential, the collector being maintained at a positive potential of 6 volts with respect to point P of the tungsten filament.

[12] Richardson, "Emission of Electricity from Hot Bodies," p. 159.

[13] L. R. Koller, Phys. Rev. **22**, 671 (1925).

The curve B was plotted from data obtained for a surface of approximately the same activity as the one corresponding to curve A. The only difference between the two cases is that the surface corresponding to curve A was obtained as a barium film was built up through evaporation from the oxide coated filaments, while the surface corresponding to curve B was obtained in the process of removing a "thick" layer of barium from the tungsten ribbon.

It is evident that the variations in I_c with the anode potential as exhibited in curve B cannot be due to change in activity. I_c is, however, also affected by other factors which are functions of the anode potential. Secondary emission from the collector and the aperture H are such factors. A third factor which appears necessary for the explanation of the great dissimilarity between curves A and B is the presence in the electron current I_c of secondary

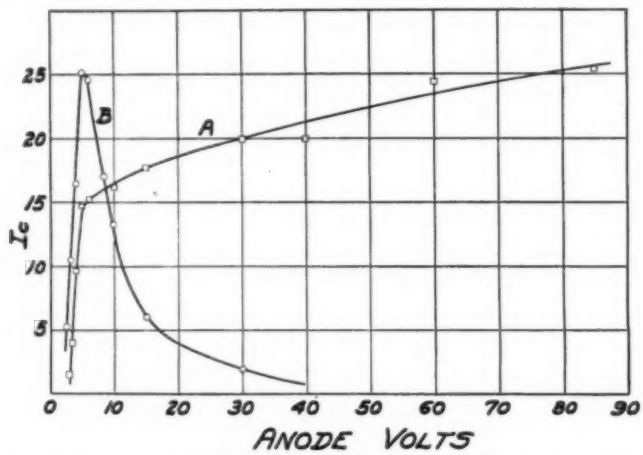

Fig. 7. The effect of the anode potential on the current to the collector at a fixed potential of the collector.

electrons which originate from points on the anode subjected to a comparatively heavy bombardment of primary electrons from the partially coated tungsten filament and then are reflected through the aperture H. Normally when the activity of the point P is greater than or nearly equal to that of the other parts of the tungsten filament, probably only a negligible fraction of I_c consists of such electrons. When points exist on the filament, however, which are of considerably higher activity than the point P it is conceivable that a large fraction of I_c consists of reflected secondary electrons. In such a case a decrease in I_c with an increase in anode potential as exhibited in curve B may be accounted for as being due to the fact that for low anode potentials the secondary emission consists largely of reflected electrons of energy equal to that of the primary electrons while for higher anode potentials the secondary emission consists largely of low velocity electrons. Since the collector is maintained at a positive potential of six volts it follows that secondary electrons which are emitted with velocities more than six volts lower than the velocity of the primary electrons will not reach the collector. Thus the fraction of the secondary electrons which have sufficient energy to reach the collector is

greater at lower anode potentials than at higher and I_c decreases as the potential is increased.[14]

Evidence of the presence of secondary electrons in I_c as discussed above may be seen in the velocity distribution curves. Curve B in Fig. 8 corresponds to a case in which the activity of the point P on the tungsten filament was considerably less than that of a point directly below the oxide filament O_1. This condition had been obtained by glowing only the filament O_1 while ordinarily both filaments were glowed to obtain a more uniform deposit of barium. The curve A corresponds to a case where the deposit was uniform. The gradual break of the curve B as compared to the sharper break of the curve A is attributed to the presence of secondary electrons.

Non-uniformities in the barium film and resulting non-uniformities in the activity along the tungsten surface apparently were produced as a result of

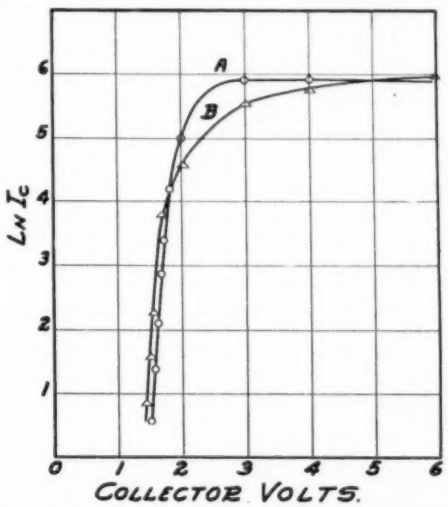

Fig. 8. To show the effect of the presence of secondary electrons on the distribution curves.

flashing the tungsten filament in removing the barium as well as a result of uneven deposit of barium in the process of evaporation.

Due to the existence of the effects discussed above, the attempt to study the relation between field intensity and activity was abandoned.

In the investigation of the relation between T_0 and V_c the assumption was made that the electron current I_c had its source at the point P. In order to make that assumption valid the data were taken under conditions where the fraction of I_c consisting of secondary electrons was negligible. A sharp break at the point O of the velocity distribution curve was taken as an indication of a low fraction of secondary electrons. For most surface conditions studied, the fraction of secondary electrons was low. Conditions corresponding to the curve B in Fig. 7 and the curve B in Fig. 8 were rare.

In conclusion, I wish to acknowledge helpful discussions during the course of this investigation with Dr. Saul Dushman and Dr. K. H. Kingdon of the General Electric Research Laboratory. I am also indebted to Dr. G. R. Shaw of this laboratory for helpful suggestions and advice.

[14] This explanation of the curve B is based upon suggestions offered by J. A. Becker.

THE EFFECT OF THE PRESENCE OF A GRID UPON CERTAIN CHARACTERISTICS OF THE AIRFLOW AT THE SURFACE OF AN AIRFOIL

By Merit Scott*
Cornell University

(Received May 18, 1931)

Abstract

In a previous article it was reported that the heat dissipation per unit area from the surface of an airfoil, as measured by resistance strips mounted parallel to the span and flush with the surface, is characteristic of the airflow. An integral relation was set up from which it was shown that the coefficient of heat dissipation is proportional to the velocity gradient at the surface of the airfoil and hence to the viscous resistance. The effect of the presence of a grid upon the above mentioned characteristics has now been observed and comprises the subject of this paper. Experimental data are presented to show the changes in the heat dissipation for different parts of the airflow due to grids of varying fineness and spacing, due to changes of angle of attack and due to changes in location of the grids with respect to the airfoil. In general, the heat dissipation is increased whenever a grid is present to induce turbulence in the air stream and the effect is maximum at about 0.6 x/c. It is concluded that near the leading edge there exists a region that serves rapidly to damp the turbulence.

ACCORDING to a development presented in an earlier paper[1] and as mentioned in the above abstract, the coefficient of heat dissipation is proportional to the velocity gradient at the surface of the airfoil and hence to the viscous resistance. This may be expressed as follows:

$$K\left[r = \mu \frac{\partial u}{\partial y_0}\right] = \left[k \frac{\partial \theta}{\partial y_0} = p_c\right]. \tag{1}$$

Wherein: r = viscous resistance per unit area; μ = coefficient of viscosity; $\partial u/\partial y_0$ = velocity gradient at surface; k = coefficient of thermal conductivity; $\partial \theta/\partial y_0$ = temperature gradient at surface; and p_c = coefficient of heat dissipation defined as the heat dissipated per unit area per degree difference in temperature between the air stream and the strip. The relation was shown to hold so long as the velocity gradient at the surface is not less than a certain limit, which might occur only in the immediate neighborhood of a stagnant point or a reversal of flow.

The effect of the presence of a grid upon these characteristics has now been observed and comprises the subject of this paper. The measurements have been made upon a symmetrical Joukowski airfoil of 4″ chord and 7″ span,

* Guggenheim Research Physicist. This work was performed in the Department of Physics at Cornell University under the direction of its committee on Aeronautic Research, supported by a grant from the Daniel Guggenheim Fund for the Promotion of Aeronautics.

[1] M. Scott, Physics 1, 48 (1931).

with nine resistance strips mounted at 0.04, 0.155, 0.25, 0.36, 0.475, 0.575, 0.69, 0.79, and 0.93 x/c. The airfoil was described and the heat dissipation characteristics presented in the former publication.[1] The mean working section velocity was maintained constant at 19.9 m/sec.

The wind tunnel, in which the measurements were carried out, is diagramed in Fig. 1. The airfoil was mounted at W and the honey comb in advance of the fan at H. After considerable preliminary testing, it was found that satisfactory conditions for these experiments were obtained by omitting the section of the tunnel ABC and closing the throat as indicated in the figure. Measurements were made with this modification. There were no deflectors or straighteners between the entrance C and the airfoil at W, but the straightener at H served satisfactorily to eliminate the angular swirling of the air stream. The span of the model was sufficiently less than that of the jet that the velocity variation across the span was not greater than 1.5 percent.

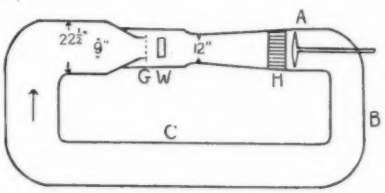

Fig. 1. Diagram of the wind tunnel.

The results of observations with several different grids are reported. These consisted of wires or screening extending across the entire jet and mounted at G(3-3/16″ upstream from the leading edge) unless otherwise stated. The specifications of these grids are as follows:

Grid No. 1 No. 14 copper wires (0.064″) spacing 1/2″
Grid No. 2 No. 14 copper wires (0.064″) spacing 1″
Grid No. 3 No. 14 copper wires (0.064″) single wire
Grid No. 4 No. 26 copper wires (0.014″) single wire
Grid No. 5 1″ mesh chicken wire
Grid No. 6 No. 14 Copper wires (0.064″) spacing 3/8″

In Fig. 2 are shown the results of measurements with grids No. 1, No. 2, No. 3 and No. 4. In all cases of single or parallel wire grids, the grids were mounted with the wires at right angles to the leading edge of the airfoil. In the case of single wires, these were mounted in the median plane of the airfoil, where the thermocouples for measurement of strip temperatures were attached to the strip.[1] At first thought one might be inclined to suppose that a grid would shield the airfoil and hence decrease the heat dissipation but this is clearly erroneous. On the contrary, the grid introduces turbulence, that is, a set of component velocities, oscillatory in character and superimposed upon those already present, characteristic of the tunnel and more particularly of that section of the tunnel at which measurements are made. This additional turbulence increases the rate of transport of momentum to the surface

and the average velocity gradient at the surface. By Eq. (1) it is to be expected therefore that the coefficient of heat dissipation should likewise be increased.

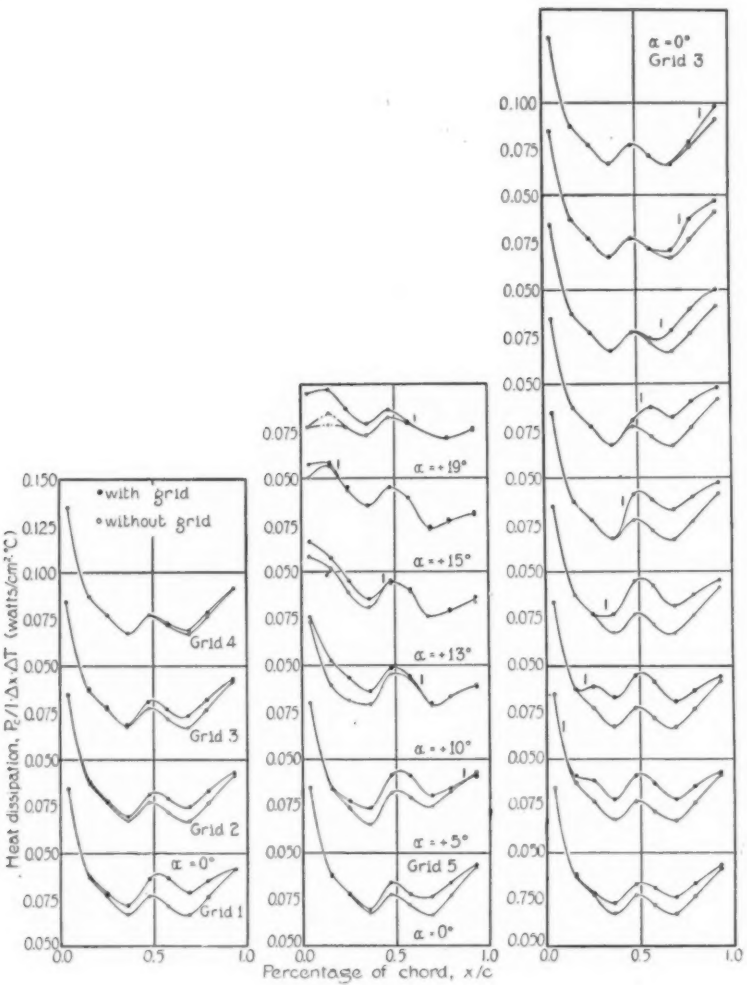

2. 3. 4.

Fig. 2. The variation of the heat dissipation coefficient with percentage of chord abscissa both with and without four different grids. Mean working section velocity 19.9 m/sec.

Fig. 3. The variation of the heat dissipation coefficient with percentage of chord abscissa, both with and without grid, the parameter being angle of attack. Mean working section velocity 19.9 m/sec. ● with grid. ○ without grid.

Fig. 4. The variation of the heat dissipation coefficient with percentage of chord abscissa, both with and without single wire grid, the parameter being position of grid as indicated by short, vertical lines. Mean working section velocity 19.9 m/sec. ● with grid. ○ without grid.

Introduction of turbulent velocity components into the hydrodynamical differential equations was made by Osborne Reynolds[2] in his attempt to

[2] O. Reynolds, Lon. Phil. Trans. (A) **186**, 123 (1895).

determine the criterion for laminar flow. H. A. Lorentz,[3] employing the same method, shows that the hydrodynamical equations for the principal motion correspond to those for the actual or turbulent motion save that the stress components have additional terms due to the transport of turbulent momentum by the turbulent velocity components. The analogy to the transport of principal momentum by molecular velocity components is inviting. It is perhaps for this reason that in certain problems an apparent coefficient of viscosity has been introduced to include the turbulent effect and whose difference from the actual coefficient of viscosity has been regarded as a measure of turbulence.

Observation of the curves of Fig. 2 shows that not all parts of the airflow at the surface of the airfoil are equally sensitive to turbulence produced in the body of the fluid upstream. The largest effect, for these particular experimental conditions, is present at a value of x/c equal approximately to 0.6.

The curves of Fig. 3 indicate the effect of the presence of a grid when the angle of attack is changed. The transitions were actually followed more closely than the representative curves of the figure show. Two features are to be noted. As the angle of attack is increased, the effect of the turbulence moves forward on the airfoil, as should be expected, in view of the fact that the stagnant point likewise moves away from the leading edge along the face (under side) of the airfoil. Any point on the back(top) of the airfoil accordingly corresponds, at higher angle of attack, to a point farther downstream so far as the flow is concerned.

The second feature is that at a certain point, as indicated by the short, vertical lines on the figure, the turbulence ceases to have any further effect. Without doubt, this point corresponds to separation of the airflow from the airfoil surface and indicates that the turbulence travels downstream without penetrating the layer of separation. This point, as observed in this way, was found to move forward to about 0.1 x/c, then jump back to a point about 0.6 x/c and gradually advance to approximately 0.4 x/c, as the angle of attack was increased from 0° to +25°.

The next series of observations refers to introducing the turbulence actually into the boundary layer next to the airfoil, using a single wire grid No. 3. The wire was located in the median plane of the airfoil, normal to its surface, and with the free end abutted to the airfoil surface. The results are given in Fig. 4, wherein the location of the grid is indicated by a vertical line neighboring the curve. In the bottom graph the grid was at the leading edge. There are several points to be noted in these data, which, for clarification, have been replotted in Fig. 5 in which the short, vertical lines indicates the leading edge.

First, the increase in the heat dissipation coefficient due to the grid in general increases (see Fig. 5) as the grid approaches the strip, then either immediately damps to zero as for strips No. 1, No. 2, No. 3 and No. 4 or more gradually decreases to zero after the grid has passed the strip. Second, the maximum effect of the grid increases, as an examination of the figure shows,

[3] H. A. Lorentz, Abh. u. theoret. Phys. p. **60**, part I_1.

with percentage of chord to a value of the latter of 0.6, then decreases. This is likewise true of the fractional maximum increase of the coefficient. Third, it is to be noted that for strips No. 5, No. 6, No. 7, No. 8, and No. 9, the effect of the grid increases rapidly (see Fig. 5) after the grid has passed the leading edge and entered the boundary layer, but this increase continues only for about 0.4 x/c, when it has reached a maximum value.

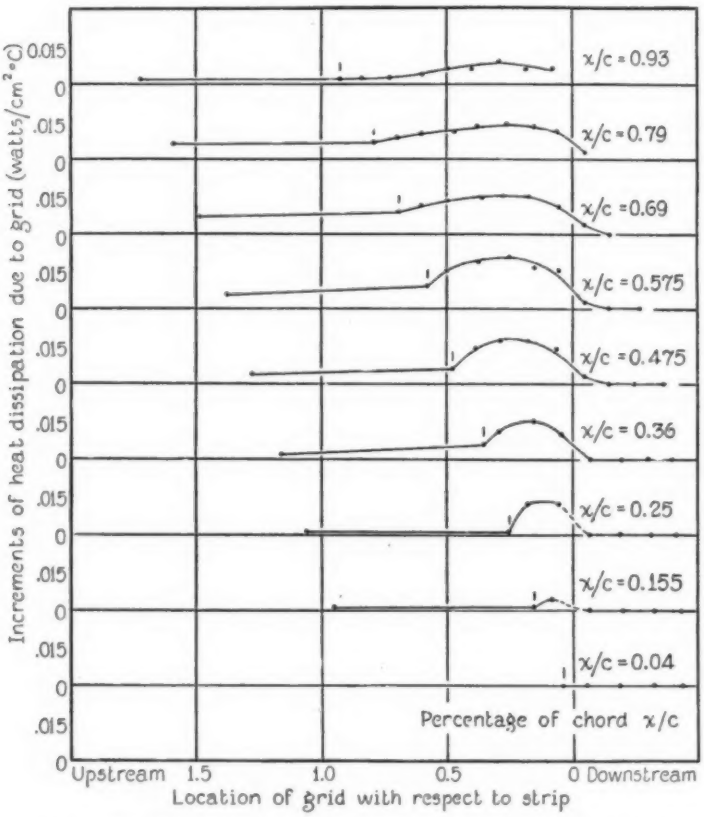

Fig. 5. The variation of the increments of the heat dissipation coefficient with location of single wire grid with respect to strip for the various strips. Data taken from Fig. 4.

The principal conclusion to be drawn is that the turbulence, induced by such grids, is rapidly damped in the boundary layer immediately downstream from the stagnant point (the leading edge in the case of angle of attack equal to zero). The damping decreases with distance back, until at about 0.4 x/c the effect seems to have vanished. The phenomenon is undoubtedly associated with and descriptive of the laminar flow in the boundary layer in the vicinity of the leading edge.

The following experiments are now described to present a more intimate view of the influence of the grids. A single No. 14 copper wire is mounted parallel to the leading edge and at a point A 3-3/16″ in advance of it, as shown in Fig. 6a. The increase in the average heat dissipation coefficient due

to it at $x/c=0.575$ (the thermocouple mounted at point C in the figure) is approximately 1.4 watts/cm²°C. If the wire is moved to point B, the effect of the grid becomes negligible. If, on the other hand, the same wire is mounted at right angles to the leading edge as at A, in Fig. 6b, the increase

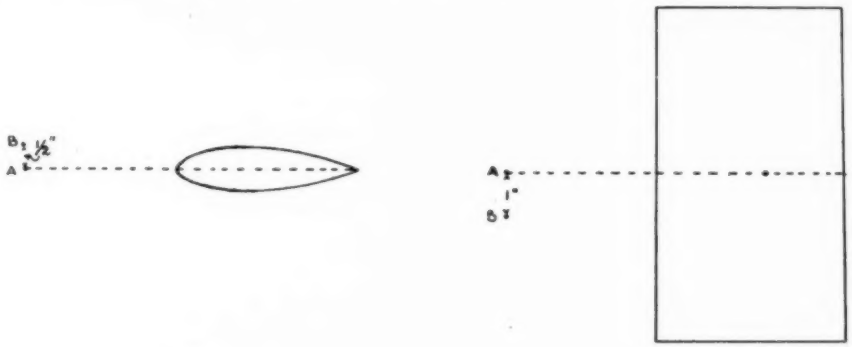

a b

Fig. 6.

in the average coefficient is only 0.5 watts/cm²·°C but the wire must be displaced about twice as much, to B, before the effect of the grid becomes negligible. Grids of No. 14 copper wire of spacings 1″, 1/2″ and 3/8″ are now interposed at the same point 3-3/16″ in advance of the leading edge and observations made with the wires parallel to the leading edge and perpendicular to it. Care must always be taken to keep the central wire in the plane of the airfoil and in the median plane respectively. The results are given in Table I wherein Δp_c is the increase in the average heat dissipation coefficient due to the grid.

TABLE I

	Δp_c watts/cm²·°C wires parallel to leading edge	Δp_c watts/cm²·°C wires perpendicular to leading edge
Single wire	1.40	0.50
1″ spacing	1.40	0.81
1/2″ spacing	1.40	1.46
3/8″ spacing	1.81	1.91

The explanation of the increase in Δp_c for the case of the grids with wires perpendicular lies in the fact that the wake of the wires does not cover the entire airfoil and the heat dissipation is increased only at those parts of the strips which lie in the wakes of the wires. The fact that Δp_c does actually become somewhat larger for the perpendicular than for the parallel wires (and this has been rather carefully verified) is presumably due to the ability of the vortices with perpendicular axes to penetrate the boundary layer more freely than those of parallel axes.

If wires of varying size are mounted perpendicularly, as at A in Fig. 6b, the result of measuring Δp_c's at $x/c=0.575$ are as shown in Fig. 7. The con-

sistency of the data for any single series without interrupting the air stream is to be noted, as shown by the dots or by the circles, whereas from one series to another, there seems to be a constant difference although the different parameters under control were maintained the same. This was characteristic

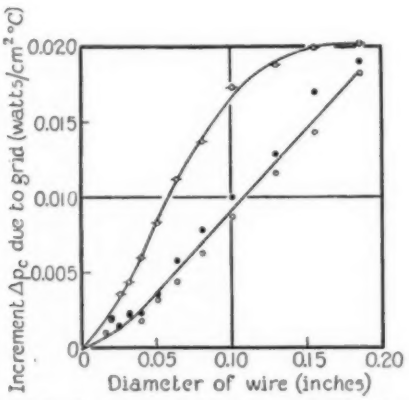

Fig. 7. The variation in the increments of the heat dissipation coefficient with radius of wire, located as at A, Fig. 7a and as at A, Fig. 7b. Dots ● and circles ○ represent single series of data without interruption of airstream, wires perpendicular. Circles with bars–○– represent single series with wires parallel.

of the work throughout. If the wires are mounted parallelly, as at A in Fig. 6b, the corresponding results are as given also in Fig. 7 by the circles with bars.

In conclusion, it may be remarked that the method herein described offers a sensitive means of observing turbulence in its relation to airfoil characteristics, and may be employed as a simple means of standardizing aerodynamic tests relative to the parameter turbulence.

PHYSICS IN THE STUDY OF PIGMENT DISPERSIONS

By F. A. Steele
The New Jersey Zinc Company, Palmerton, Pennsylvania

(Received May 25, 1931)

Abstract

The study of colloids has reached the point where many important contributions are coming from physicists. Even more attention from physicists will be required if this science is to progress as it should. A suitable dispersion of zinc oxide in kerosene has a high yield value and marked plastic properties. A few drops of a dispersing agent added to this mixture largely destroys its plastic properties and greatly increases its fluidity. It is well established that the dispersing agent accomplishes this result by decreasing the interfacial tension and thereby destroying the flocculation of the pigment. In certain cases in paints, however, there is reason to believe an entirely different phenomenon is responsible for yield value and plasticity. Much work with the tools of the physicist is indicated in the solution of this problem. There is much to be done in the study of solid-liquid interfacial tension, adsorption layers, interfacial potentials, and the dielectric properties of colloids before these problems are to be solved. The behavior of pigments in rubber is also discussed.

THE study of colloids has passed through the various stages which are common to most sciences. Once the general principles underlying colloid phenomena were discovered, the more salient features of a great number of different colloid systems were studied and described. Empirical rules for preparing, studying, and describing these systems were evolved, and the quantity of more or less disconnected data which came to exist was quite overwhelming. Then, gradually, came the tendency to return to the more simple systems and study them exhaustively. With this reaction came new methods of experimental attack and new viewpoints on the most fundamental and established principles of the science. As these expermental methods and these new viewpoints became more and more fundamental, they tended to change, as always, from those traditional to the chemist to those traditional to the physicist. Many colloid chemists became physicists and some physicists became interested in colloids. The latter was probably the more efficient transition; it is easier to apply familiar methods to unfamiliar problems than unfamiliar methods to familiar problems. The contributions of certain physicists to the field of colloids have been notable.

Pigments are used in paint and rubber largely to influence the chemical and mechanical properties of the systems. The problems arising in the study of these disperse systems are probably more numerous and complex than would be expected by the uninitiate. While much progress has been made in the manufacture and application of these pigments, many of the most fundamental properties of the dispersions are not at all well understood. The writer wishes to present a few of these problems to the group which this publication will reach, with the hope that perhaps a few physicists will become

sufficiently interested to apply their talents to these most interesting and important questions.

When a mixture of a nonpolar oil, such as kerosene, and zinc oxide is prepared in suitable proportions, a highly plastic material is formed. This paste has a relatively high yield value and is capable of very little elastic deformation; under higher stresses it flows continuously. Such properties would hardly be conceivable if every particle were completely surrounded with liquid; as a matter of fact, it is not. The free energy of the interface is so high that a decrease in free energy results when the solid particles approach closely enough to one another to eliminate some of the interface. In a dilute suspension this process would result in a clumping of the pigment; that is, the pigment would be flocculated. In this concentrated paste the pigment forms an essentially continuous structure in which distortion involves what amounts to solid-to-solid friction. Thus is the yield value and the absence of marked elasticity explained.

If a few drops of a surface active material, such as stearic acid, be added to the mixture, it will concentrate at the interface, lower the interfacial tension, and reduce or eliminate the tendency of the pigment to flocculate. Thus each particle becomes entirely surrounded with a true liquid layer and the yield value disappears or at least is reduced to a different order of magnitude. These phenomena are well-known and the theoretical analysis of them is well substantiated and quite generally accepted. There are, however, other pigment-liquid mixtures with somewhat similar properties, which have received no such satisfactory theoretical treatment.

A suitable ferric hydroxide-water gel, which has a considerable yield value, may be transformed to a sol by shaking and changed back to a gel by by being allowed to stand. This phenomenon is called thixotropy. Such a system differs in properties from the kerosene-zinc oxide mixture in two important respects. First, if stress in excess of the yield value has been applied to the ferric hydroxide sol, a sensible length of time is required for the yield value to be regained while in the case of the zinc oxide-kerosene mixture the regain is essentially instantaneous; and, second, the ferric hydroxide sol is capable of a marked elastic deformation while the other system is not. While these differences may be a matter of degree rather than kind, it is evident that the theory which was so satisfactory for one system can hardly be applied to the other. A system whose yield value is the result of essentially solid to solid friction could not give the large elastic deformation under a stress below the yield value that is characteristic of a gel; and it seems hardly probable that much time could be consumed in assuming a stable flocculated structure in a medium so fluid as water when it is considered that the change in the position of each individual particle in going from a completely dispersed to a flocculated state would be only a micron or so. And, to add to the confusion, even though a satisfactory theoretical treatment of the gel were available, there are systems with border-line properties which could not, at present, be ascribed definitely to either class.

One hypothesis has been widely advanced to cover elasticity and yield

value in thixotropic gels. In a word, this hypothesis supposes the existence of an adsorbed layer of dispersing medium around each solid particle so thick that relative motion of the particles is impossible without at least partial destruction of the adsorbed layer. The elasticity inherent in this envelope accounts for the elasticity of the gel and the time required for the formation of the layer accounts for the duration of the sol state. This picture fits the facts well enough to have gained considerable cognizance. The difficulty lies in the fact that the existence of this envelope has never been conclusively demonstrated; has never, in fact, so far as the writer is aware, been shown to be compatible with what is known about the molecular forces and the kinetics involved.

To account for the data that have been published by some workers[1] the adsorbed layer of water around the micelles in certain gels would have to be some microns thick. If these water molecules are fixed firmly enough to form a structure of the observed mechanical strength, the phenomenon should be accompaied by certain other effects. In the first place, the constraint of so many molecules would be expected to be accompanied by marked heat effects, and certainly the heat capacity of the constrained water should be lower than that of the free liquid. Some data on these effects would be very helpful at the present time.

It has also been pointed out that polar molecules so constrained should respond less readily to an electrostatic field than those of the free liquid, thus reducing the dielectric constant of the material. Since the molecules in the adsorbed layer are not in a truly solid condition but more likely simply have a much increased relaxation time, this effect should be especially pronounced at high frequencies. A number of attempts have been made to determine the bound water in certain systems but most of them have been concerned with systems like gelatine which are a bit beside the present discussion. An excellent paper by Kistler[2] has appeared very recently, however, on the dielectric constants of Fe_2O_3, Al_2O_3, and bentonite sols. These sols are all non-thixotropic; that is, they will not gel if they are sufficiently free of electrolyte. Now Kistler made the very surprising observation that these sols had dielectric constants indistinguishable from that of water in the non-thixotropic state but that the di-electric constant was lowered when they were rendered thixotropic by the addition of electrolyte, *whether the measurement was made on the sol or the gel.* The decrease in the dielectric constant was a function of the amount of electrolyte added but was constant for a given material whether it was measured as a gel or a sol. This is a most striking observation and it is very desirable that this work be checked by some other worker and extended to other systems.

The writer, in collaboration with Mr. S. E. Kamerling, made a sporadic attempt to obtain some dielectric constant data on thixotropic and non-thixotropic paints nearly a year ago. The experimental difficulties were hardly overcome in the time available and no conclusive data were obtained. The

[1] E. A. Hauser, Kolloid-Z. **48,** 57 (1929).
[2] S. S. Kistler, J. Phys. Chem. **35,** 815 (1931).

study of non-aqueous systems offers certain advantages as well as certain difficulties that are not found in water dispersions. Any well substantiated data in this field would certainly be a valuable contribution.

Early in this paper a statement was made in regard to the relationship between flocculation and interfacial tension. In many cases it is difficult to determine whether the tendency to flocculate has been increased or decreased by an alteration in a disperse system which has resulted in a change in its physical properties. For instance, certain small changes in the composition of a pigment-vehicle mixture may greatly alter its flow characteristics under very small stresses. Whether this is a result of a change in interfacial tension with a consequent change in the flocculating tendency or to a change in the thickness of the adsorbed layer, is frequently quite impossible to establish. A method whereby solid-liquid interfacial tensions could be determined would be of enormous value here as in other phases of surface chemistry. Failing this, the determination of differences in interfacial tension from one system to another would be a big step. It is recognized, of course, that the difficulty in determining the tension of the solid-liquid interface is much the same as that of determining the surface energy of the solid, a problem which has received the attention of a number of physicists. There are, however, a number of possibilities which may in time lead to some valuable data on this problem.

Bartell and Osterhof[3] have designed an apparatus whereby it is claimed that adhesion tension measurements can be determined. This makes it possible, in certain cases, to determine the difference in the interfacial tension between two liquids and the same solid. There has been some question as to the validity of the data obtained by this method, however, and the difficulty has not been entirely cleared up.

There are two other possible attacks which might shed some light on this problem. Koch[4] has derived the formula,

$$\Delta e = \frac{2\sigma M}{r\rho nF}$$

where Δe is the difference in potential between a spherical particle of radius r and a plane surface of the same material and σ is the interfacial tension between the material in question and the liquid in which it is immersed. Since the other variables in the equation are capable of experimental determination, the surface tension could be calculated. Although this expression is closely related to the change of solubility with interfacial tension, the experimental approach would be quite different. The practicability of this method would be well worth investigating.

In many systems flocculation and dispersion are reversible phenomena; that is, a flocculated system will disperse spontaneously if the interfacial tension is sufficiently reduced, and vice versa. Where the interfacial tension is so low that no particles adhere upon collision, the dispersion is complete.

[3] Bartell and Osterhof, Ind. & Eng. Chem. **19**, 1277 (1927).

[4] F. K. V. Koch, Phil. Mag. Sup. **2**, 585 (1931).

When, however, the interfacial tension is somewhat larger, the tendency to flocculate due to the adhesion of the particles must reach an equilibrium with the tendency of the particles to disperse due to their thermal agitation. It should be possible to formulate the energy relationships involved at equilibrium and, by experimentally determining the degree of dispersion, to calculate the interfacial tension. To the writer's knowledge, no such approach to the problem has been made.

There are many problems in connection with the dispersion of pigments in rubber that might well receive the attention of physicists, but the field can only be touched upon here. The addition of pigments, such as zinc oxide and carbon black, to rubber causes a marked reinforcement in the cured stock; that is, a pigmented stock has a stiffer stress-strain curve and requires a greater total energy to break than an unpigmented stock. A great deal of work has been done in this field, but the facts still remain without a satisfactory explanation. The separate effects of particle size, particle shape, and the specific properties of the material composing the pigment have never been adequately treated. This situation is probably the result of poor fundamental approach as well as the inherent experimental difficulties attending quantitative studies of rubber compounds.

One example of faulty approach to this problem may be worth mentioning, largely because the theory which it involves seems to be receiving more general acceptance than the facts justify. The theory is based upon the following statement by Hock,[5] "Man hat gefunden, dass diese verstärkende Wirkung der aktiven Füllstoffe, zu denen z.B. Russ and Zinkoxyd gehören, um so auffälliger hervortritt, je feiner die Füllstoffe sind. Die Benetzung von Kautschuk und Füllstoff is also offenbar die Ursache der Verstärkung. Sucht man auf diesen Grundvorstellungen eine Theorie der Kautschukfüllstoffe zu entwickeln, so hat man offenbar die freie Grenzflächenenergie zwischen Kautschuk und Füllstoff für die Vergrösserung der Zerreissarbeit verantwortlich zu machen." From this standpoint is the theory developed. Hartner,[6] having devised a method for estimating the total free energy of the pigment-rubber interface, gets an order-of-magnitude check with the increased energy to break. The point which both of these workers seem to have overlooked is that this free surface energy can be of primary importance in reinforcement, only if the interface changes in magnitude or character during elongation and break. It has been established experimentally many times that the former change does not take place, and there is no reason to believe that the latter does. As a matter of fact, Hartner seems to assume that the entire rubber-pigment interface is destroyed when the test piece is ruptured, an obviously erroneous assumption. This case is cited as an example of the many practical problems concerning the properties of pigment dispersions which would doubtless progress more rapidly if they could receive the benefit of the experimental technique and method of attack of the physicist.

[5] L. Hock, Z. Elektrochem. **34,** 662 (1928).
[6] F. Hartner, Kolloidchem. Beihefte **30,** 83 (1929).

THE ELECTRIC CONDUCTIVITY AND CAPACITY OF DISPERSE SYSTEMS

By Hugo Fricke

The Walter B. James Laboratory for Biophysics
The Biological Laboratory, Cold Spring Harbor, L. I.

(Received June 12, 1931)

Abstract

This report refers in particular to suspensions of biological cells. The interior of a biological cell is a well-conducting salt solution, but at its surface polarization or the presence of a nonconducting membrane obstructs the passage of an electric current with a resulting low conductivity and high dielectric constant of the suspension. The theory for the passage of an alternating current through a suspension of this type is dealt with and experimental work with various kinds of suspensions such as cream, wet sand, blood, and animal tissue, is described to show the applicability of the theory. The determination of the volume concentration of suspensions, of the form factor of the suspended particles, of the thickness of surface membranes, and of the interior conductivity of living cells, are instances of practical applications.

THIS report includes a group of investigations which have been made during the last few years.[1] The work was done with a special interest in biological usage, but applies as well to a wider field.

The first measurements of the electric resistance of living cells were made in the middle of the foregoing century. Such well-known physicists as Peltier, Weber, v. Humboldt, and Lenz worked in this field. A large amount of work was done by the noted physiologist du Bois Reymond, who summarized the work done up to 1850 in his "Untersuchungen über tierische Elektrizität."

The fundamental fact was brought out that a living cell becomes polarized when an electric current passes through it, the resistance of living matter being, in consequence, high when a direct current or a current of low frequency is employed, but decreasing when the frequency is increased. Very little of lasting value was accomplished, however, before the advent of the audion oscillator made the production of alternating currents of pure form and of different frequencies a simple matter.

For theoretical study, we may take as a simplified model a suspension of conducting particles, at the surface of each of which polarization of the electric current takes place. Consider first the conductivity of a suspension of homogeneous, non-polarizable spheres. The theoretical solution of this problem was given by Maxwell in his "Treatise on Electricity and Magnetism." He derived the well-known formula:

$$\frac{(K/K_1)-1}{(K/K_1)+2} = \rho \frac{(K_2/K_1)-1}{(K_2/K_1)+2} \qquad (1)$$

[1] Phys. Rev. **24**, 575 (1924); **25**, 361, (1925); **26**, 678, (1925); **26**, 682, (1925).
Jour. Gen. Physiol. **6**, 741 (1924); **9**, 137 (1925); **9**, 153 (1925).
Jour. Cancer Res. **10**, 340 (1926).

where K = Specific conductivity of suspension; K_1 = Specific conductivity of suspending liquid; K_2 = Specific conductivity of suspended particle; and ρ = Volume concentration of suspended material, which in the field of conductivity is usually referred to as Maxwell's formula, but which is known under other names in other departments of physics, such as the Lorenz-Lorentz formula, the Clausius-Mossotti formula, or the Poisson formula.

I have tested this formula over a wide range of volume concentrations by working with cream. A heavy cream was obtained by separating raw, fresh milk in a De Laval cream separator. The conductivity of this cream, of

TABLE I. *Test of Maxwell's formula for the conductivity of a suspension of spheres.*

	Volume concentration percent	
	Calc. from resistances	Calc. from dilution factors
Primary cream	62.73 ± .12	62.93 ± .19
Dilution No. 1	40.40 ± .08	40.44 ± .12
Dilution No. 2	22.49 ± .06	Standard

the skimmed milk, and of various mixtures of the two were measured. Table I shows the result of such a series. One column gives the volume percent of the fat particles calculated from Maxwell's formula, which in this case reads:

$$\frac{K}{K_1} = \frac{1-\rho}{1+\frac{1}{2}\rho} \tag{2}$$

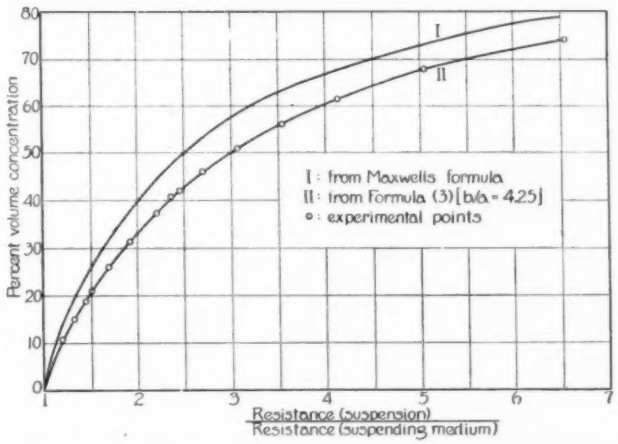

Fig. 1. Resistance of suspensions of red corpuscles of different concentrations.

where K = Conductivity of cream; K_1 = Conductivity of skimmed milk; and ρ = Fat-content of the cream. The next column shows the relative volume concentration calculated from the dilution factor.

Much work has been done on the conductivity of blood. The red corpuscle is a non-conductor and therefore the conductivity of blood is lower than the conductivity of the serum.

How well does Maxwell's formula apply to a suspension of red corpuscles? In Fig. 1 are plotted experimental data obtained with red corpuscles of a dog.

The ordinates indicate volume concentration, and the abscissas the ratio of conductivities of serum to corpuscle-suspension. The upper curve is calculated from Maxwell's formula. The reason for the deviation is that the form of the corpuscle of mammals is far removed from the spherical shape, it being that of a flat, biconcave disk.

It is a fairly simple matter to extend Maxwell's formula to the case of a suspension of spheroids. The following formula is obtained:

$$\frac{(K/K_1) - 1}{(K/K_1) + X} = \rho \frac{(K_2/K_1) - 1}{(K_2/K_1) + X} \tag{3}$$

where X depends on K_2/K_1 and on the axis ratio a/b of the spheroid, but is independent of the volume concentration ρ. X is shown graphically in Figs. 2 and 3 for the oblate spheroid and the prolate spheroid, respectively. When $a/b = 1$, we have $X = 2$, which is the Maxwell formula.

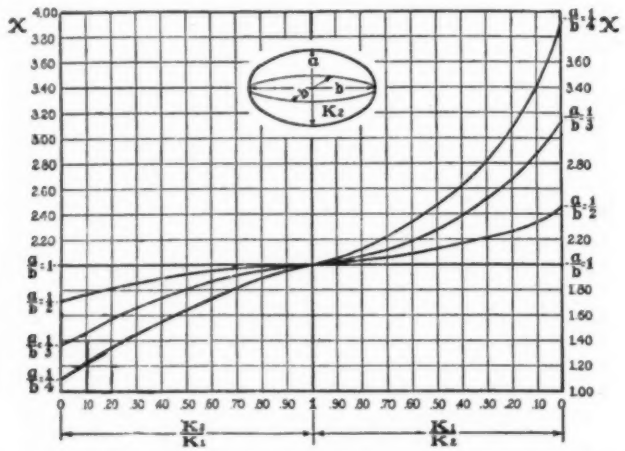

Fig. 2. Graphical representation of x for the case of the oblate spheroid.

The curve II in Fig. 1 has been calculated from formula (3), using $a/b = 1/4.25$, which gives $X = +1.05$. The agreement is very satisfactory; in fact, it is rather surprising that the agreement is so good at the highest volume concentrations, where the corpuscles are packed far beyond the limit set by the total packing factor, indicating that deformation of the cells must have taken place. There has been much discussion about what the form of a red corpuscle is when it is in the blood. It is, of course, not certain that the form we observe microscopically is the true form, and it has been insisted, from various sides, that it is not. In the microscope the corpuscle is seen to be of the form of a biconcave disk. The ratio of diameter to maximal thickness for the dog is between 3 and 5. Our value $a/b = 1/4.25$ indicates this to be the true form.

As a precision method for determining the red corpuscle volume, the conductivity method is not wholly satisfactory for mammals, because the form of the corpuscle is not an ellipsoid. But for the lower orders—birds, fish, reptiles—the shape is ellipsoidal and the conductivity method should give

results of highest exactness. The method is often used in physiological investigations and might be useful also in practical clinical work if a simple apparatus for this particular use were placed on the market. The conductivity method may also be useful for the practical determination of the fat content of milk and cream, although no attempt of so using it has been made as yet. Other possible fields of practical application are the determination of rubber in latex and the analysis of soils.

TABLE II. *Conductivity of suspensions of sand.*

k_1/k (obs.)	ρ (obs.) (percent)	x (calculated)
1.190	10	1.410
1.426	20	1.420
1.734	30	1.405
2.156	40	1.367
2.715	50	1.400
3.613	60	1.35
	Average value	1.392

Table II shows some measurements of the conductivity of suspensions of sand, which were made in Wilhelm Ostwald's laboratory many years ago. The

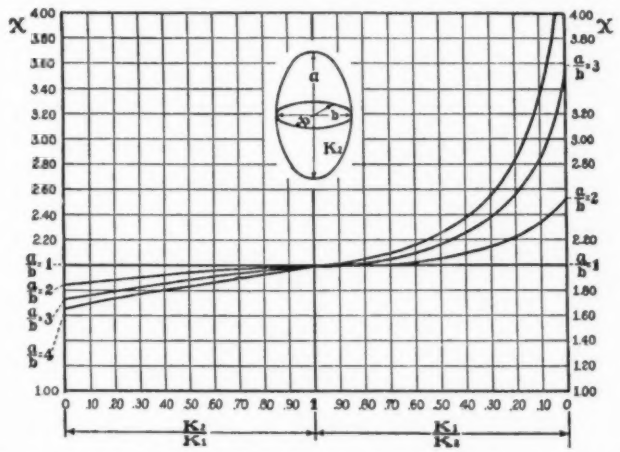

Fig. 3. Graphical representation of x for the case of the prolate spheroid.

suspensions were made by adding the sand to hot salt solutions containing 3 percent gelatine and cooling this mixture to gelatination under continuous rotation. The concentrations vary from 10 percent to 60 percent. I have applied formula (3) to these measurements, for each concentration calculating X, using the experimental values of K_1/K and ρ. The values of X stay perfectly constant. As X is smaller than 2, the sand particles must have been flat. The average ratio of a/b is about 1/3.

For a current of low frequency the living cell is practically a nonconductor, due to polarization at its surface. In order to obtain the true conductivity of the cell, a current of high frequency must be used. This is illustrated by data shown in Table III. Here are given measurements of the resistance of calf

TABLE III. *Capacity and resistance of blood of calf for frequencies from 87,000 to 4½ million cycles.*

Cycles per sec. ($\omega/2\pi$).	Capacity (mmf)	Resistance (ohms)	$\frac{146}{1+(146\cdot 10^{-12}\cdot\omega\cdot 370)^2}$	$\left[\frac{1}{370}\,\frac{(146\cdot 10^{-12}\cdot\omega\cdot 370)^2}{1+(146\cdot 10^{-12}\cdot\omega\cdot 370)^2}+\frac{1}{191}\right]^{-1}$
87,000	146	191	146	191
833,000	130	181	135	183
$1.17\cdot 10^6$	118	174	126	178
$1.52\cdot$ —	106	168	115	172
$2.04\cdot$ —	90	159	98	163
$3.04\cdot$ —	68	148	71	151
$3.82\cdot$ —	60	144	55	144
$4.52\cdot$ —	39	138	43	140
		(124)	—	126
∞	—	extrapolated		

blood with currents of different frequencies. The resistance at infinite frequency is extrapolated to be 124 ohms, while at low frequency the resistance is 191 ohms. Using formula (3) with $a/b = 1/4.25$, the value of 124 ohms leads to a value for the specific resistance of the corpuscle as follows:

$$\frac{\text{spec. res. corpuscle}}{\text{spec. res. serum}} = 3.5.$$

It may be noted that the high resistance of the red corpuscle, which is recorded when the frequency is low, seems to be due not to a polarization at its surface but to the presence of a thin nonconducting membrane around the corpuscle. The interior of the corpuscle is a well-conducting salt solution. At a sufficiently high frequency the impedance of the static capacity of the membrane becomes negligible; the resistance of the red corpuscle calculated above representing the resistance of the interior of the corpuscle. By this method a continuous record may be made of the exchange of electrolytes between the serum and the corpuscle interior,—a problem of considerable physiological importance.

The polarization which takes place when an electric current is sent through living cells makes itself felt when we try to measure the resistance of the cells in a bridge. It is impossible to obtain an equilibrium without adding a certain amount of capacity in parallel to the resistance in the opposite arm of the bridge. For small current densities, a suspension of living cells is electrically equivalent to a resistance in parallel to a capacity [Fig. 4(c)]. The value of this parallel capacity we term the capacity of the suspension. The capacity of a cm cube of the suspension is the specific capacity. The specific capacity of animal or vegetable tissues, such as liver, muscle, roots or fruits, is usually quite large—several thousand micromicrofarads at 1000 cycles—while the specific resistance is a few thousand ohms. The measurement of the capacity for such material is very simple. Suspensions of single cells, such as blood or bacteria, usually have much lower capacities. Since their resistance is low, the exact measurement of the capacity is a more difficult matter. For

instance, the specific capacity of the blood of man, which is due to the red corpuscles, is a few hundred micromicrofarads, while the specific resistance is about 150 ohms. Table IV shows measurements at different frequencies of the

TABLE IV. *Resistance and capacity of suspension of red corpuscles of chicken.*

Kilocycles per second	Resistance	Directly measured capacity (Micromicrofarad)	Capacity measured for salt solution (Micromicrofarad)	Capacity due to polarization at electrodes (Micromicrofarad)	Capacity of corpuscles (Micromicrofarad)
1/2	4080	366	+46	56	321
1	4080	340	+12	20	328
2	4080	317.5	−4	7	320.5
4	4080	307.5	−14.5	2.5	322
8	4073	298.5	−17	1	315.5
16	4022	293.5	−20	0	313.5
32	3924	293.5	−16	0	309.5
64	3664	274	−16.5	0	290.5
128	3072	231	−16	0	247
256	2324	173.5	−16	0	189.5

Temperature: 18.30°C
Cell constant: 2.58
Specific resistance: 1582 ohms
Specific capacity: 825 micromicrofarads.
Specific resistance of serum. 92.8 ohms.
Specific capacity for 100 percent suspension: 878 micromicrofarads.

capacity of a concentrated suspension of red corpuscles of chicken made with a Wheatstone bridge. The first column gives the resistance, the next the capacity directly recorded in the bridge. The next column gives the capacity measured when the electrolytic cell was filled with a salt solution of the same resistance as the corpuscle suspension. The difference is the capacity due to the red corpuscles. The capacity of the salt solution increases at low frequencies due to electrode polarization. I have chosen this example to show the influence of electrode polarization. However, for accurate results we should use electrolytic cells so large that the electrode polarization is negligible.

Consider a suspension of conducting spheroids, each being covered with a thin nonconducting membrane. The specific capacity of the suspension at low frequency is expressed by the following formula:

$$C = \alpha \cdot \left(1 - \frac{K}{K_1}\right) \cdot q \cdot C_0 \qquad (4)$$

where K = Conductivity of the suspension; K_1 = Conductivity of the suspending medium; q = Major axis of the spheroid; C_0 = Static capacity of one sq. cm of the membrane; and α = Depends on the axis ratio of the spheroid, and its values are shown in Table V.

TABLE V. *Values of α as a function of b/a and of a/b.*

b/a	1	2	3	4	∞
α	1.50	1.30	1.27	1.28	1.65
a/b	1	2	3	4	∞
α	1.50	1.03	0.94	0.94	$(0.118 \times a/b)$

Axis of spheroid a, b, b,

We may write formula (4) as follows:

$$C = C_{100\%} \cdot \left(1 - \frac{K}{K_1}\right)$$
$$\text{With } C_{100\%} = \alpha q C_0. \tag{5}$$

where $C_{100\%}$ is a constant, which may be considered as the capacity of a 100 percent suspension. This formula shows that the capacity varies as $1 - K/K_1$, in its dependence on the volume concentration. In this form, the formula is independent of the form of the spheroid and may be applied to a suspension of particles of any form.

This formula has been tested by measuring the capacity of suspensions of red corpuscles of different concentrations. Table VI shows the results of a

TABLE VI. *Capacity of suspensions of red corpuscles of dog in own serum.*

No. of experiment	Volume concentration calculated from resistance	Resistance (r) (ohms)	Capacity (C) mmf	Capacity (C_{100}) for 100 percent concentration (calculated)	Origin
	percent				
I	83.9	931.	374	411	Concentrated by centrifugation from original blood.
II	21.0	126.9	129	385	From 83.9 percent suspension by dilution.
III	72.0	498.	343	411	From 83.9 percent and 21. percent suspensions.
IV	47.5	230.2	237	374	From 72.0 percent suspension by dilution.
V	60.2	329.	286	385	From 83.9 percent and 47.5 percent suspensions.

Resistance of serum: 84.25 ohms.

series of such measurements. By formula (5) $C_{100\%}$ is calculated from the observed values of the capacity C. The values of $C_{100\%}$ are constant from 21 percent to 84 percent concentration.

Using formula (4) we find the capacity per cm² of the corpuscle surface $C_0 = 0.80 \mu f$, the value obtained being the same for corpuscles of man, rabbit, calf, dog, chicken and turtle.

An interesting fact about the red corpuscle is that its capacity is independent of the frequency of the electric current. The capacity also stays constant when the corpuscle is suspended in different media which do not change its form, such as a sodium chloride solution or a sugar solution. These facts favor the assumption that the capacity represents an actual static capacity of a thin non-conducting surface membrane. If we assume this to be true and choose a suitable value for the dielectric constant of this membrane we may estimate its thickness. With $C_0 = 0.80 \mu f$ and the dielectric constant 3, we find the thickness to be 40.10^{-8} cm.

Formula (4) holds only when the frequency is so low that the impedance of the capacity of the membrane is large compared with the resistance of the

cell interior. When the frequency is increased to such a point that this is not the case, the resistance and capacity of the suspension decrease. With good approximation this decrease may be calculated as follows: Fig. 4 (a) shows the suspension schematically. A part of the electric current passes between the cells and encounters the resistance R_0. A part passes through the cells and

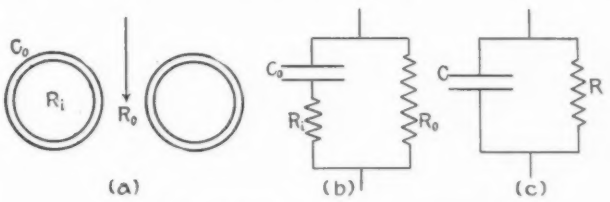

Fig. 4. Electrical diagram of a suspension.

encounters the capacity of the membrane C_0 and the resistance R_i, which is the resistance of the cell interior. Thus, electrically, the suspension may be represented by the diagram (b). The capacity and resistance of the suspension are defined by diagram (c). The following equations are easily derived:

$$C = \frac{C_0}{1 + (C_0\omega R_i)^2} \tag{6}$$

$$\frac{1}{R} = \frac{1}{R_0} + \frac{1}{R_i}\cdot\frac{(C_0\omega R_i)^2}{1 + (C_0\omega R_i)^2} \tag{7}$$

C_0, R_0, and R_i are all directly observable: R_0 is the resistance measured at low frequency; C_0 is the capacity measured at low frequency; $(1/R_0+1/R_i)^{-1}$ is the resistance at very high frequency.

Table III contains at different frequencies measurements of the resistance and capacity of a suspension of red corpuscle, and the values calculated by formulae (6) and (7). The agreement is quite satisfactory.

Usually the capacity of living cells is due to a polarization at the cell surface. The polarization acts as a capacity in series with a resistance and the resistance and capacity of the suspension may be expressed by formulae (6) and (7) by using:

$$R_i = R_p + R_i^1$$
$$C_0 = C_p$$

where R_p is the polarization resistance, R_i^1 the resistance of the cell interior, and C_p the polarization capacity. Thus the following formulae are obtained:

$$\frac{1}{R} = \frac{1}{R_0} + \frac{C_p\omega R_i + m}{1 + (C_p\omega R_i + m)^2}C_p\omega \tag{8}$$

$$C = \frac{C_p}{1 + (C_p\omega R_i + m)^2} \tag{9}$$

$$m = C_p\omega R_p.$$

For low frequencies when R_i is negligible compared with the impedance of the polarizations capacity, the equations may be written:

$$\frac{1}{R} = \frac{1}{R_0} + C\omega m \tag{10}$$

$$C = \frac{C_p}{1 + m^2} \tag{11}$$

Experience shows that m is independent of the frequency, or at least approximately so, a law which is known to hold also for the polarization at metal electrodes in aqueous solutions.

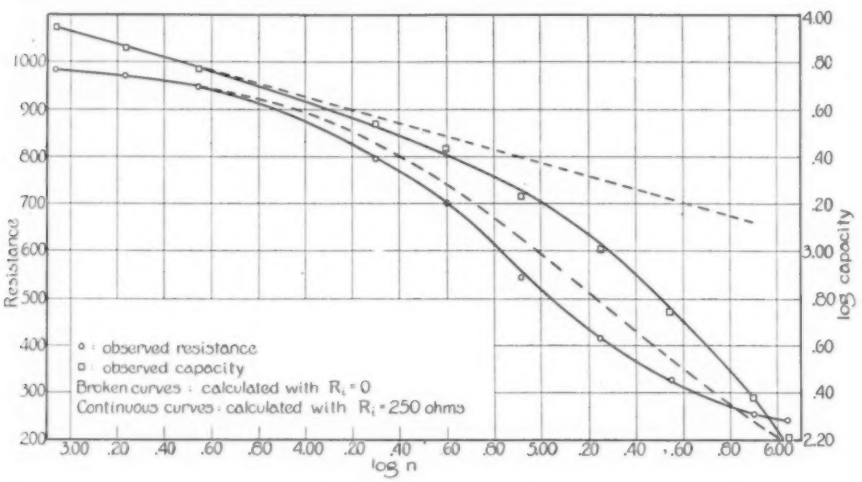
Resistance
log capacity
log n
o : observed resistance
□ : observed capacity
Broken curves : calculated with $R_i = 0$
Continuous curves : calculated with $R_i = 250$ ohms

Fig. 5. Resistance and capacity of muscle of rabbit for currents of different frequencies.

The points in Fig. 5 represent measurements of the resistance and capacity of a piece of rabbit muscle. The decrease of the resistance at low frequencies is due solely to the polarizations resistance, and may be accounted for by formula (10). Hereby m may be calculated. We find $m = 0.46$. By formula (11) C_p may now be calculated, and thereafter by using formula (4), the value of the polarization capacity per cm² of cell surface may be calculated.

It has been found for the polarization at the so-called polarizable metal electrodes that the polarization capacity varies nearly exponentially with the frequency $C_p \sim \omega^{-z}$, and this same law is found to hold also for polarization at cell surfaces. The exponent falls between 0 and 1/2 and is usually about 0.30. In this particular case it is 0.28.

The broken curves in Fig. 5 have been calculated by formulae (10) and (11), without considering the resistance of the cell interior, using $m = 0.46$ and taking C_p to vary as $\omega^{-0.28}$. The resistance of the cell interior makes its influence felt at about 5000 cycles. The fully drawn curves have been calculated with $R_i = 250$ ohms. The agreement is very satisfactory.

The measurement of the polarization of living cells is one of the important physical methods for obtaining information about the nature of cell mem-

branes. It should also be noted that the existence of polarization forms a criterion for the presence of living cells, which in some cases may be of use when optical methods fail. It is a significant fact that the polarization seems to be of the same type as is observed at so-called polarizable metal electrodes in aqueous solutions, e.g. platinum in sulphuric acid. Since it seems certain that definite potentials are maintained across cell membranes, one might have expected to observe the type of polarization which is produced at the so-called non-polarizable metal electrodes as silver in silver nitrate and which is characterized thereby that the polarization capacity varies inversely as the square root of the frequency. But apparently the mechanism by which the bioelectrical potential is maintained is too slow to be effective within the period of one cycle of the alternating current.

THREE METHODS OF STUDYING CAPILLARY STRUCTURE AS APPLIED TO WOOD

By Alfred J. Stamm, Chemist
Forest Products Laboratory,[1] Forest Service
U. S. Department of Agriculture

(Received May 20, 1931)

Abstract

Three different physical methods for studying the capillary structure of porous materials are developed and applied to the study of the fine effective continuous capillary structure of wood. The three characteristic capillary properties measured are, (1) the ratio of effective capillary cross section to the effective length, (2) the average effective capillary radius, and (3) the maximum effective capillary radius. Some of the important characteristics of the porous structure of wood are briefly presented in order to show that the major part of the void structure, the fiber cavities, have very little to do with the permeability of wood. The pores in the pit membranes which connect the adjacent fiber cavities are shown to be the structure effective in controlling permeability of wood. The pores in the pit membranes in general, are below microscopic visibility, thus necessitating other means of study. The ratio of the effective capillary cross section to the effective capillary length is determined from electrical resistance measurements of strong salt solutions filling the void structure and from the specific resistance of the salt solutions in bulk. Strong salt solutions are used in order to make the surface conductivity negligible as well as the conductivity of the swollen cell wall. The average effective capillary radius is determined by combining the results of the preceeding measurements with results obtained from hydrostatic flow studies of a continuous water phase extending through the section. Poiseuille's law is used for the calculations. A differential pressure drop apparatus was devised for these measurements in which the flow of liquid through a standard capillary tube and the test specimen connected in series is determined by measuring the pressure drop through each. The maximum effective capillary radius is determined by measuring the gas pressure required to overcome the effect of the surface tension of water in the capillary systems. The data show the large differences between the fine capillary structure of heartwood and of sapwood.

THE study of the capillary structure of porous materials is not only of theoretical interest but also of considerable practical importance. For example, a more nearly complete knowledge of the fine capillary structure of wood should lead to better seasoning practice, improved impregnation with preservatives, and improved penetration of chips in chemical pulping processes.

Variations in the coarser capillary structure of wood, notably the fiber cavities, the pores, and the resin ducts, which make up the major part of the porosity of wood, have been shown to effect the permeability but slightly. On the other hand, the permeability of two specimens that have a coarse capillary structure practically identical may differ tremendously. (Table II).

[1] Maintained at Madison, Wis., in cooperation with the University of Wisconsin.

This is due to the fact that the fiber cavities are closed at both ends, the only communication from fiber cavity to fiber cavity being through the membranes of the bordered pits or through the cell wall. It is the size and also the number of the finer openings that control the permeability of wood.

Fig. 1 shows a photomicrographic section of a typical softwood cut across the fibers. A bordered pit connecting two adjacent fiber cavities appears in cross section below the center of the figure. The openings, approximately

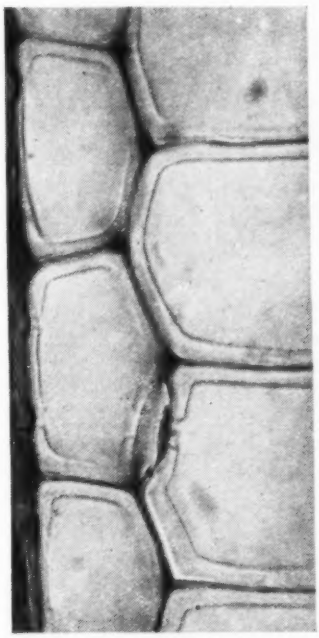

Fig. 1. Cross section of wood (×1000) showing an aspirated bordered pit connecting two adjacent fiber cavities.

circular in shape, in the adjacent cell walls are separated by a membrane that is a continuation of the middle lamella—the cementing material between the fibers. This membrane, particularly with softwoods, has a slight central thickening called the torus. In some cases the pits are aspirated, that is the torus is held against one of the seats of the cell wall opening, thus making the pit act like a closed valve (Fig. 1).

The permeability of a pit will depend upon its condition. If the pit is not aspirated, the permeability will be a function of the porosity, the area, and the thickness of the membrane. If it is aspirated, the permeability will further depend upon how closely the valve seat fits and whether it is cemented in a closed position with resinous material.

Consideration of the fact that Fig. 1 is magnified to the limit of reasonable definition makes obvious the additional fact that an examination of photomicrographs will give little information on permeability. Such a method of study is eliminated also by the large number of measurements that would have to be made. Each softwood fiber with an average length of about 0.3 cm

and a diameter of approximately one hundredth of this value has from 30 to 300 pits connecting it to adjoining fibers, and there are from 50,000 to 100,000 of such fibers in a square centimeter of cross section.

The fine capillary structure of wood, however, can be fairly well characterized by a combination of three different types of physical measurements. In the previously reported researches from this Laboratory on capillary structure of wood, the effective continuous capillary cross section was determined indirectly by means of electroendosmotic flow measurements.[2,3] This method has recently been abandoned because it is involved and requires several approximations. The ratio of the effective capillary length to the effective continuous capillary cross section is now being determined by measuring the electrical resistance of strong salt solutions in the wood structure and in bulk.[4,5] An average effective capillary radius (fourth root of the average fourth power) is determined by combining the effective capillary values with data obtained by pressure-permeability measurements of a continuous water phase extending through the wood sections, using Poiseuille's law.[2,3] The maximum effective capillary radius is determined by measuring the gas pressure required to overcome the effect of the surface tension of water in the capillary systems.[2,3] An additional method of study, consisting of measurements of the permeability of the wood to colloidal solutions containing particles of approximately known size, serves as a check upon the capillary sizes obtained by the two previous methods. Since no recent measurements by this method have been made, the method will be dismissed here with the statement that it has always given results consistent with those of the other methods.[2,3,6]

The data presented in this paper will be confined to the simplest case, coniferous woods and transverse sections in which the flow of electric current, flow of water, and displacement of water are all in the direction of the fiber length. The specimens were all cut from fresh, unseasoned wood.

Determination of the Ratio of the Effective Capillary Length to the Effective Continuous Capillary Cross Section by an Electrical Conductivity Method

The ratio of the effective capillary length to the effective continuous capillary cross section can be calculated from the electrical resistance of the wood sections, the voids of which are completely filled with a salt solution, and from the specific resistance of the salt solution in bulk, providing the surface conductivity is made negligible and the conductance of the cell wall is negligible. The surface conductivity for very dilute salt solutions and especially for distilled water may be many times the bulk conductivity of the solution or of the

[2] Stamm, Colloid Symposium Monograph **6,** 83 (1928).
[3] Stamm, J. Agr. Research **38,** 23 (1929).
[4] Fairbrother and Mastin, J. Chem. Soc. **125,** 2319 (1924).
[5] Marshall, J. Soc. Chem. Ind. **48,** 373T (1929).
[6] Bechold & Szidon, Kolloid Z., Special No. April 1, 259 (1925); McBain and Kistler, J. Phys. Chem. **35,** 130 (1931).

water,[3,4,5,7,8] but for appreciable salt solution concentrations this surface conductivity becomes negligible in comparison with the bulk conductivity. When the potassium chloride solutions used in this investigation exceeded a concentration of 0.07 mols per 1, the ratio of the specific resistance of the salt solution in bulk to its resistance in the wood structure was found to be independent of concentration, thus indicating that the surface effects are negligible. Hence, measurements were made using salt solutions exceeding this concentration.

The specific conductance of dry wood is extremely small, approximately 10^{-12} mho on an over-all dimension basis. When water is adsorbed by the cell wall the conductivity increases so as to give a linear relationship between the logarithm of the conductivity and the moisture content, up to fiber saturation, at which point the specific conductance is 3×10^{-6} to 1×10^{-5} mho.[9] The water adsorbed in the cell wall at this point shows an increased conductivity over the bulk conductivity of water, because of surface conduction. Salt solutions, however, act differently. The conductivity of such solutions

Fig. 2. Diagramatic representation of the capillary path through wood showing the manner in which the fiber cavities are connected through the pores of the pit membranes.

at the fiber-saturation point, although exceeding that for water, is sufficiently less than the bulk conductivity to make the conductivity of the cell wall in the presence of the salt negligible for the present measurements. This is due to the fact that salt solutions are not dispersed in the cell wall substance in a continuous manner as with water, but are confined to the grosser capillary spaces; this fact will be considered more at length in a later publication.

The electrical conductivity of a transverse wood section, the capillary structure of which is filled with a salt solution, is thus substantially equal to the sum of the bulk conductivities of the solution in all of the individual capillary paths connected in parallel. These capillary paths in turn are made up of fiber cavities and pores of pit membranes connected in series (Fig. 2). The part of the electrical resistance for which the fiber cavities are responsible can be calculated from the fractional void volume or average fractional capillary cross section of soaked swollen wood, q, which in turn can be obtained from the bulk density d of the wood on a wet volume and dry weight basis. and the density of wood substance, d_0 which is equal to 1.52.

Thus,

$$q = 1 - \frac{d}{d_0}. \tag{1}$$

[7] D. R. Briggs, J. Phys. Chem. **32,** 641 (1928).

[8] McBain, Peaker and King, J. Am. Chem. Soc. **51,** 3294 (1929); McBain and Peaker, J. Phys. Chem. **34,** 1033 (1930).

[9] Stamm, Ind. Eng. Chem. Anal. **1,** 94 (1929).

The value of q obtained in this way includes the voids in the cell wall, which as already shown are electrically ineffective, as well as the fiber cavity voids and other void structure which, for this purpose, is negligible. The fractional void volume or average fractional void cross section of the cell wall is equal to the product of the moisture content M per gram of dry wood at the fiber-saturation point, and the density of the wood, d. The average fractional cross section of the fiber cavities,

$$q_f = q - Md \tag{2}$$

and the electrical resistance of the fiber cavities

$$R_f = \frac{R_{sp}L}{(q - Md)Q} \tag{3}$$

where R_{sp} is the specific resistance of the salt solution, L the thickness of the section under investigation, and Q the cross section of the specimen.

The total resistance R_m of the salt solution in the pores of the pit membranes will depend upon the fractional cross section of such pores traversed in parallel and the length of path, that is, the continuous effective capillary cross section q_m of the pores expressed as a fraction of the cross section of the

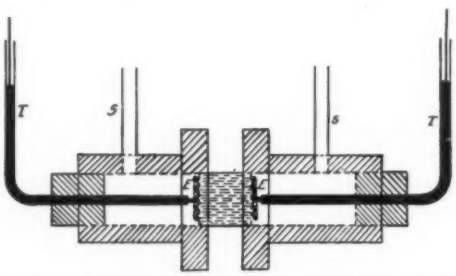

Fig. 3. Cells used in electrical resistance measurements.

specimen, and the sum l_m of the thicknesses of the pit membranes traversed in series. Then,

$$R_m = \frac{R_{sp}l_m}{Qq_m}. \tag{4}$$

The experimentally measured resistance R is equal to the sum of the resistances from Eqs. (3) and (4).

$$R = \frac{R_{sp}L}{(q - Md)Q} + \frac{R_{sp}l_m}{Qq_m} \tag{5}$$

and

$$\frac{l_m}{q_m} = \frac{Q}{R_{sp}}\left(R - \frac{R_{sp}L}{(q - Md)Q}\right). \tag{6}$$

The measurements were made upon cylindrical sections of wood that had been turned in a lathe in a soaked and swollen condition to fit tightly into

the ends of two hard-rubber cells (Fig. 3). Two sets of cells and electrodes for sections of 0.665 cm² and 2.66 cm² cross-sectional area were used. The electrodes E are heavy platinum wire disk coils sealed into glass tubes T that are filled with mercury for electrical contact. The electrodes were freshly platinized each day before using. The side tubes S are for convenience in filling with liquid. The measuring apparatus consisted of a student circular slide-wire bridge, a 4-dial resistance box (0.1 to 999.9 ohm), a microphone hummer, telephone receivers, a condenser, a switch, and dry cells connected according to standard conductivity measuring practice.

The sections were soaked in distilled water for at least two weeks. To facilitate the replacement of air by water the soaking was done in a vacuum desiccator to which suction was applied intermittently. Potassium chloride was then added. Electrical resistance measurements on the wood sections showed that diffusion was complete and equilibrium of the salt distribution was obtained in less than a week. The specific resistance of the salt solution in equilibrium with the wood sections was determined, using the hard-rubber cells of Figure 3 clamped together with a ring gasket replacing the wood section. Measurements were made with the electrodes separated by different distances. The measurements were made at 25°C in a thermostatic air bath.

TABLE I. *Ratio of the effective capillary length to the effective continuous capillary cross section obtained from electrical resistance measurements at 25°C.* KCl conc. = 0.79N, R_{sp} = 9.84 ohms, M = 0.30.

Specimen	l	q	Q	L	R	R_f	l_m/q_m
Slash pine Heartwood	0.430	0.717	2.66	1.965	15.30	12.40	0.783
	0.430	0.717	2.66	1.450	11.30	9.13	0.587
	0.430	0.717	2.66	.922	7.20	5.81	0.375
	0.430	0.717	2.66	.585	4.68	3.69	0.267
	0.430	0.717	.665	1.925	59.90	48.50	0.771
	0.430	0.717	.665	1.400	43.80	35.30	0.575
Slash pine Sapwood	0.456	0.700	2.66	1.940	15.00	12.75	0.608
	0.456	0.700	2.66	1.365	10.65	8.97	0.453
	0.456	0.700	2.66	.960	7.38	6.30	0.292
	0.456	0.700	2.66	.640	5.05	4.20	0.229
	0.456	0.700	.665	1.890	58.50	49.80	0.588
	0.456	0.700	.656	1.395	43.00	36.70	0.426

The data for both the sapwood and the heartwood of slash pine are given in Table I and plotted in Fig. 4. Within the range of experimental error the straight lines pass through the origin as would be expected according to theory. The linear relationship indicates that q_m the continuous effective capillary cross section, varies but slightly for the adjoining sections and that l_m, the total length of the effective capillaries, varies directly with the thickness of the sections, thus indicating a rather uniform distribution of the effective capillaries. Such a relationship is rather to be expected, considering the large number of fiber cavities and pit membranes traversed by the current. It is rather surprising, however, that the difference between the sapwood and the heartwood is so small. This fact can be better understood after consideration of the other capillary methods.

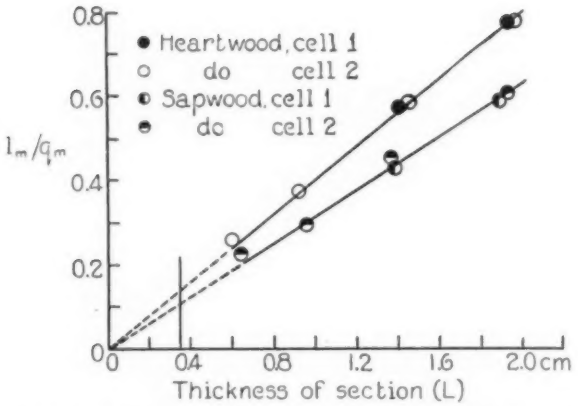

Fig. 4. Relationship between the ratio of the effective capillary length to the effective capillary cross section and the thickness of the section.

An approximation of the actual value of q_m can be made by taking the value of l_m/q_m from the graphs for a section whose thickness is equal to that of half the average fiber length (0.175 cm) and taking the thickness of a single pit membrane, which was found microscopically to range from 2×10^{-5} to 2×10^{-4} cm. Dividing l_m by l_m/q_m gives a value of q_m ranging from 3.6×10^{-4} to 3.6×10^{-3}. This is in as good agreement with the value of q_m obtained by electroendosmosis[2,3] as could be expected, because of the uncertainty of the effective value of l_m.

Determination of the Average Effective Capillary Size by Means of Hydrostatic Flow Studies

In the capillary flow of liquids under hydrostatic pressure the velocity is dependent not only upon the total continuous effective capillary cross section but also upon the effective size of the individual ducts. By combining the previous data for the ratio of the effective capillary length to the effective continuous capillary cross section with data from hydrostatic-flow studies, it becomes possible to calculate the actual size of the average effective capillary openings. The passage of liquids under external pressure through a smooth capillary tube of circular section for conditions of stream-line flow (which are obtained for the capillary systems considered, a correction for impact turbulence alone being necessary[2,3]) may be quantitatively expressed by Poiseuille's law[2,3,15]

$$V = \frac{\pi r^4 P}{8\eta l} = \frac{A r^2 P}{8\eta l} \tag{7}$$

in which V represents the rate of flow, r the capillary radius, l the capillary length, P the applied pressure, η the viscosity of the liquid, and A the cross-

[15] Reynolds, Roy. Soc. (London) Phil. Trans. **174,** 935 (1883); Biglow, J. Amer. Chem. Soc. **29,** 1675 (1907); Bartell, J. Phys. Chem. **16,** 318 (1912); Bartell and Carpenter, J. Phys. Chem. **27,** 252 (1923); Hitchcock, J. Gen. Physiol. **9,** 755 (1926).

sectional capillary area, all in c.g.s. units. For a bundle of N capillaries Eq. (7) becomes,

$$V = \frac{N\pi r^4 P}{8\eta l} = \frac{Qqr^2 P}{8\eta l} \tag{8}$$

where Q is the total cross section of the bundle of capillary tubes and q is the fractional open cross section. In this case r is the fourth root of the average fourth power of all of the radii rather than an arithmetic average. Since the range in size of the pores of the pit membranes is not great as explained in the following section of this article, the value will not differ appreciably from the arithmetic average.

Instead of determining the volume of discharge of water from the capillary system per unit of time under a definite head, with the system held at a constant temperature so that η is both determinable and constant, a differential method, which involves several special features, was used. If the section under test and a calibrated capillary tube are connected in series with

$$V_1 = \frac{Qq_1 r_1 P_1}{8\eta l_1} \tag{9}$$

for a test section where q_1, r_1, and l_1 represent the effective fractional cross section, effective radius and effective length, and

$$V_2 = \frac{\pi r_2^4 P_2}{8\eta l_2} \tag{10}$$

for a calibrated standard capillary tube then since

$$V_1 = V_2 \tag{11}$$

$$r_1 = \left(\frac{\pi r_2^4 l_1 P_2}{Q l_2 q_1 P_1}\right)^{1/2} \tag{12}$$

The question arises as to what constitutes the effective cross section, effective radius, and effective length for hydrostatic flow through the broken capillary system of wood. This question is answered by a simple experiment of Ewert[11] who found that under a head of 80 cm of water 4.0 to 4.2 cc of water flowed per hour through a capillary tube having a radius of 0.0075 cm and a length of 8 cm; the theoretical flow for these conditions was 4.3 cc per hour. The tube was then cut into 16 lengths of 0.5 cm and each length was sealed into a tube 0.2 cm in radius and 5 cm long. All of these units were connected in series, thus giving a discontinuous capillary analogous to the capillary path through a section of wood. Under the same head of water, 3.8 to 3.9 cc passed through the tube per hour, showing substantially that only the fine capillaries are effective in determining the rate of flow and that the rate is practically the same as for one capillary with a length equal to the sum of the lengths of the sections, the small variation being accountable for on the basis of increased impact turbulence, which is corrected for in this investigation.

When the frictional resistance in the fiber cavities is negligible in com-

[11] Ewart, Roy. Soc. (London) Phil. Trans. (B) **198**, 41 (1905).

parison with that in the pores of the pit membranes, as it was in the preceding illustration, the effective dimensions q_1, r_1, and l_1 are equal to the corresponding dimensions q_m, r_m, and l_m of the pores of the pit membranes. Eq. (10) then becomes

$$r_m = \left(\frac{\pi r_2^4 l_m P_2}{Q l_2 q_m P_1}\right)^{1/2}. \tag{13}$$

Where the resistance to flow through the fiber cavities is not negligible in comparison with the resistance through the pit membranes, Eq. (10) assumes a more complicated form

$$\frac{1}{\frac{\pi r_2^4 P_2}{l_2}} = \frac{1}{\frac{Q q_f r_f^2 P_1}{L}} + \frac{1}{\frac{Q q_m r_m^2 P_1}{l_m}} \tag{14}$$

and

$$r_m = \left(\left(\frac{l_m}{q_m}\right)\frac{1}{\left(\frac{Q l_2 P_1}{\pi r_2^4 P_2} - \frac{L}{q_f r_f^2}\right)}\right)^{1/2} \tag{15}$$

where q_f and r_f are for the fiber cavity dimensions, and L is the thickness of the section. q_f is equal to $(q - Md)$ as in Eq. (2) and r_f is the average radius of the fiber cavity estimated from Table 10 of the previous paper.[3]

The apparatus used for these measurements is shown in Fig. 5. It consists essentially of three tubular glass compartments, I, II, and III, separated by means of the wood section M and the standard capillary tube C. A new clamping device D is made of brass and is fastened to tubes I and II with de Khotinsky cement. Rubber gaskets are used on each of the clamp faces. This clamping device not only has the advantage over the previously used type in forming a tighter seal, but also in preventing evaporation from the edges of the section. Mercury manometers P_1 and P_2 indicate the pressure drops between compartments I and II; and II and III, respectively. Where the resistance to flow through the standard glass capillary is very small as compared to that through the wood section, thus giving a very small pressure drop across P_2, the manometer P_2 is replaced by an inverted water manometer, thus increasing the accuracy of reading 12.6 times. A is the intake and B the over-flow. The tubes S are merely for convenience in filling the apparatus with water and displacing the air. A constant hydrostatic head of water is applied at A. When the pressure drops through the standard capillary and the wood section came to equilibrium, which required several hours for resistant heartwood sections but only a few minutes for the sapwood sections readings on the manometer tubes were recorded. Reversing the connections so that the hydrostatic head is applied at B on the standard capillary side rather than on the wood-section side, with A serving as the over-flow, has no effect upon the equilibrium pressure-drop ratio.

The pressure-drop ratio P_2/P_1 is not constant for different applied heads, as would be expected for an ideal system free from turbulence. This deviation from constancy was shown to be due to impact turbulence at the ends of the

capillary tubes.[2,3] The impact turbulence is a function of the velocity of flow and of the length of the capillary (see Couette's amplification of Poiseuille's equation[12]) and becomes negligible for infinitesimal applied heads. Hence, it can be eliminated by determining P_2/P_1 for a number of different applied heads and extrapolating to zero applied head. This correction is explained more in detail in an earlier publication.[2,3]

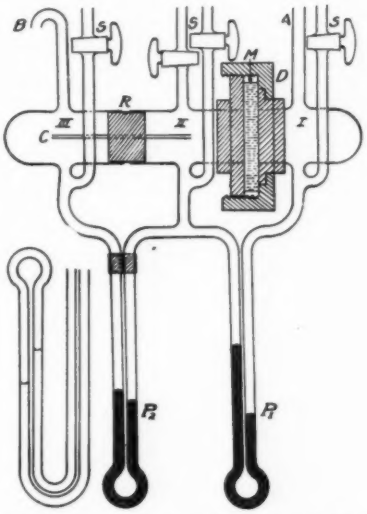

Fig. 5. Differential pressure-drop hydrostatic-flow apparatus.

For these measurements it is extremely important to displace all of the air from the sections. This was done by intermittently applying suction in a vacuum desiccator to the sections immersed in water. Heating the water to 60°C facilitated the removal of air. This treatment in all cases was continued for at least two weeks.

TABLE II. *Effective capillary sizes from hydrostatic flow and from the overcoming of surface tension.* $Q = 2.08$ cm² (for hydrostatic flow), $r_f = 0.001$ cm.

Specimen	L	r_2^4/l_2	l_m/q_m from Fig. 4	P_2/P_1 (extrapolated)	r_m	p	r^{max}
					Cm	*Kg*/cm²	*Cm*
Slash pine Heartwood	1.340	0.53×10^{-9}	0.54	0.013	2.37×10^{-6}	27.0	5.5×10^{-6}
	0.875	.53	0.35	0.025	2.65	22.0	6.7
	.670	.53	0.27	0.037	2.83	15.5	9.5
	.670	3.73	0.27	0.0047	2.66	—	—
						Cm of mercury	
Slash pine Sapwood	1.980	32.1×10^{-9}	0.62	1.25	2.19×10^{-4}	12.0	9.0×10^{-4}
	1.365	32.1	0.43	1.70	2.11	11.2	9.7
	0.915	32.1	0.29	2.40	2.04	10.2	10.6
	.730	32.1	0.23	2.85	1.97	9.5	11.4

[12] Herschel, Colloid Chemistry, Theoretical and Applied **1**, 727 (1926) edited by Alexander Chemical Catalog Co., New York.

The average effective radii of the pit-membrane pores of the heartwood and the sapwood of slash pine are given in Table II. With heartwood, the pit membranes are alone effective in resisting flow, whereas with sapwood the fiber cavities are also partially effective. The differences in the effective pore sizes for these two parts of the same wood are rather large.

Determination of the Maximum Effective Capillary Size by Overcoming the Effect of Surface Tension with Applied Gas Pressure

The determination of the pressure required to overcome the effect of surface tension in the capillary system permits the calculation of the maximum effective capillary diameters, using Jurin's law.

Liquids with a density d that wet capillary tubes with an angle of wetting θ rise in the tubes to a height h dependent upon the radius of the tube r, the surface tension of the liquid σ, and the counter pull of gravity g. Equilibrium is reached when the resultant force F is equal to zero. Hence,

$$F = \pi r^2 hdg - 2\pi r\sigma \cos\theta = 0 \tag{16}$$

and

$$\sigma = \frac{rhdg}{2\cos\theta} \tag{17}$$

For water and other liquids that wet the capillaries completely, θ is equal to zero and the expression simplifies to,

$$\sigma = \frac{rhdg}{2}. \tag{18}$$

When σ is known for the liquid used, this equation serves as a means of determining r by merely measuring h. This method, however, can not be used with wood capillaries because their opacity prevents the measurement of h and also because the irregularity of the capillary systems makes it practically impossible to bring the menisci to the points desired for measurement. Although h is not directly measureable, the pressure ρ that will just cause the removal of the liquid from a capillary, thus overcoming the effect of surface tension, can be readily determined.[13] Since

$$\rho = hdg \tag{19}$$

then

$$r = \frac{2\sigma}{\rho}. \tag{20}$$

If several capillaries of different bores are combined in a bundle, water will be displaced first from the tube of least capillary resistance, which will be the tube having the maximum effective bore, the effective bore being the minimum bore for a capillary of nonuniform cross section.

[13] Biglow and Bartell, J. Amer. Chem. Soc. **31,** 1194 (1909); Bartell, J. Phys. Chem. **16,** 318 (1912); Bartell and Carpenter, J. Phys. Chem. **27,** 252 (1923).

The apparatus used for these measurements is shown in Fig. 6. It consists of a *T* tube made of brass, with a flange on one arm for clamping wood sections securely over the open end of the arm. The disk plate that holds the wood section in place by means of four screws has in it several small holes distributed over the area of the tube to allow the free passage of air, while still supporting the section sufficiently to prevent rupture from taking place readily at high pressures. Rubber gaskets are used between the flange and the wood section and between the plate and the wood section so as to make the seal practically air-tight. For wood sections of low resistance the gas pressure was obtained from the laboratory compressed-air supply line and the pressure applied was measured on a mercury manometer. For resistant sections a tank of oxygen under high pressure, having a readily controllable needle valve, formed the source of gas pressure and the pressure applied was measured by means of a calibrated pressure gauge, which was sensitive to 0.5 Kg.

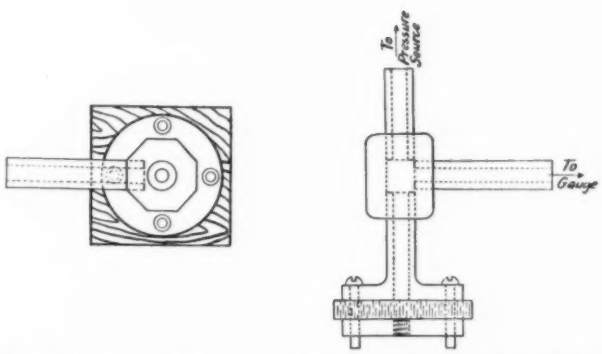

Fig. 6. Apparatus for overcoming the effect of surface tension.

The measurements were made on water-soaked sections that were clamped securely between the flange and the plate, and dipped into a dish of water just far enough for the liquid to touch the bottom of the wood section. The gas pressure was applied gradually, so as to allow for complete dissipation, and the pressure at which the first gas bubbles emerged from under the immersed plate was observed. It is readily possible to distinguish actual passage of gas through the section from the slight gas leak between the non-immersed flange and the wood; leaks of this nature can not be entirely eliminated at higher pressures. The possibility of distinguishing the two kinds of gas flow makes this type of flange connection preferable to the cup type used with the previously described apparatus. After making a determination the apparatus was disconnected from the pressure line and a drop of water was placed in the tube to assure the resoaking of the upper part of the section; then after standing for a few minutes a check determination was made.

The right-hand part of Table II gives the results of these measurements, made at approximately 25°C, for the same heartwood and sapwood sections of slash pine used for the hydrostatic flow measurements. The value for the maximum effective pore radius in each case decreases with an increase in

thickness of the section. This is to be expected; the most effective path through a number of pit membranes in series will approach the average effective path as the number of pit membranes in series increases, because of the decreasing probability of all the pit membranes in series containing pores of maximum size. Measurements made by this last method of study upon radial sections, in which the tangential displacement of water by gas is through the same structure except that far more pit membranes are traversed in series, gave values of r for the heartwood of 4.0×10^{-6} cm and for the sapwood of 3.7×10^{-4} cm. The number of pit membranes traversed in series for these sections was approximately 40, whereas the number traversed for the sections of Table II was from 2 to 5.

Conclusions

Data obtained by the three methods used for studying the capillary structure of wood indicate that there is a large difference in permeability between the heartwood and the sapwood of slash pine; that of the sapwood is 4,000 to 5,000 times that of the heartwood. This difference in permeability is not due to a difference in the effective continuous capillary cross section but rather to the difference in the size of the effective openings. The radii of the maximum effective openings range from 3 to 6 times the corresponding average values. The values for the size of the effective openings obtained by the method of overcoming the effect of surface tension approach the average values in the case of thick sections where the number of pit membrnaes traversed in series is large. The fact that two entirely different methods of measuring the size of the effective openings give results of the same order of magnitude serves as a check upon the validity of the methods.

Summary

1. Three physical methods for studying capillary structure have been developed and applied to the study of the fine structure of wood.

2. The ratio of the effective capillary length to the effective continuous capillary cross section is obtained from the electrical resistance of salt solutions filling the wood structure and the specific resistance of the solutions in bulk.

3. The average effective capillary radius is obtained combining data from the preceding measurements with data obtained from hydrostatic-flow studies of a continuous liquid phase extending through the wood sections, using Poiseuille's law. A differential pressure-drop apparatus was devised for these measurements, in which the flow of liquid through a standard capillary tube and the test specimen connected in series is determined by measuring the pressure drop across each.

4. The maximum effective capillary radius is determined by measuring the gas pressure required to overcome the effect of the surface tension of a liquid in the capillary systems.

5. Data obtained by these methods show the large difference between the fine capillary structure of heartwood and of sapwood.

SOME COLLOIDAL PROPERTIES OF BENTONITE SUSPENSIONS

By H. A. Ambrose and A. G. Loomis
Mellon Institute of Industrial Research and Gulf Research Laboratory, Pittsburgh, Pa.

(Received April 27, 1931)

Abstract

A study of the swelling and gelling properties of bentonite dispersions has been made in connection with the increasing use of this mineral for drilling oil wells. It is shown that the emulsoid type of colloids present responds to changes in the *pH* of the dispersion medium with respect to rate of settling, viscosity and swelling, thus behaving as a typical hydrophilic colloid. The curve for percent of solid matter settled in a definite time as ordinate against the *pH* shows a maximum at the isoelectric point, with minima on each side of this point, corresponding to the points of maximum adsorption. As the *pH* is further increased or decreased flocculation begins with increased rate of settling. The viscosity curve is closely related to the rate of settling curve, showing maxima and minima corresponding to the electro-viscous effect. Maximum swelling occurs at approximately the point of maximum viscosity. Methods are given for controlling the swelling of bentonites. Relaxation curves are given for bentonite suspensions and utilized to explain the suspension qualities of these sols for heavy mineral dispersions, such as barytes or amorphous silica. A few applications of bentonite sols to the drilling of oil wells are given.

I. Introduction

THE examination of the properties of bentonite suspensions is of interest on account of its swelling and gelling properties, together with its multitude of industrial uses.[1] In this connection our particular interest is the use of the mineral in rotary drilling fluids for sinking oil wells. By virtue of their colloidal properties natural and prepared bentonites are having an increased application in the technique of oil-field drilling, both as protective colloids for the stabilization of suspensions and alone in water as a self-contained drilling fluid. Any drilling fluid may be considered as a three-component system: water, gel-forming colloids, and non-gel-forming colloids. Of these two types of colloids the gel-forming type is by far the more important, for this group is responsible for the necessary characteristics of a drilling fluid, i.e. viscosity, suspension, body or consistency, lubrication, sealing and gel properties in general. Colloids of the non-gelling type, together with larger particles, contribute partially to the viscosity but more particularly to the specific gravity of the drilling fluid. The understanding of the proper use of bentonite in drilling fluids demands a knowledge of the properties of the gel-forming colloids in particular. We have, therefore, examined natural and treated bento-

[1] Davis and Vacher, Bur. Mines Tech. Paper **438**; Alexander, Colloid Symposium Monograph **2**, 99 (1925).

nite for the purpose of gaining a clearer comprehension of the physical and chemical properties of this mineral with respect to its emulsoid content and how this type of colloid may be chemically and physically controlled to have maximum efficiency for the practical use under consideration.

II. Properties of Bentonite

Certain bentonites of high colloidal content have astonishing powers of imbibition. A 5 percent dispersion in water will swell and form a stiff gel, occupying a volume twenty times the original volume of the solid mineral. Small percentages of bentonite added to clay dispersions that have lost their quality of low settling rate, due to loss of colloidal material, will restore these qualities, and the viscosity of the suspension is considerably increased. This finds practical application in restoring spent clay drilling fluids that have lost their colloids in porous formations. A clay dispersion requires about ten times as much weight of solid material in suspension as a bentonite dispersion to have the same viscosity as the latter.

In drilling through formations of high gas pressure weighted drilling fluids are necessary to furnish the required hydrostatic head to balance this pressure. Heavy minerals such as barytes are used for this purpose, but the suspension qualities of such materials are poor. A small percentage of bentonite added to such suspensions will entirely arrest the tendency to settle by virtue of the protective action of the bentonite colloids.

III. Origin and Occurrence of Bentonite

The principal commercial deposits of bentonite with high content of colloids are in South Dakota, Wyoming and California. It appears that the mineral is a decomposition product of volcanic ash.[2] There are several reasons comprising this evidence, such as the absence of quartz, which is present in all ordinary clay sediments, the presence of feldspar, and the extension of individual beds over great distances without much variation in thickness. The clayey matter in normal sediments has been so acted on by electrolytes and other active substances that it has lost its original porosity and tendency to imbibe water with attendent swelling, which bentonite exhibits to such a marked degree. The chemical composition of bentonite is, moreover, exactly what one would expect from the partial alteration of an intermediate igneous rock, accompanied by the removal of alkalies and addition of water.

Bentonites are probably hydrated silicates of aluminum, according to Davis and Vacher,[3] and may be represented by the formula $Al_2O_3 \cdot 4SiO_2 \cdot \times H_2O$. Some bentonites appear to contain about 50 percent of particles of colloidal size (5–200mμ). According to Wherry[4] the colloidal properties of bentonite are due to a "felted" texture, the particles crystalline, of colloidal thickness, but of appreciable size in the other two dimensions. The adsorptive capacity for water is supposedly due to the wetting of these flat surfaces

[2] Hewett, J. Wash. Acad. Sci. **7**, 196 (1917); Wherry, ibid. 576.
[3] Reference 1.
[4] Wherry, Am. Mineral. **10**, 120 (1925).

by adsorbed water. The properties of gel formation by bentonite suspensions is probably due to the interlocking of crystals when the suspension is at rest.

IV. Experimental Work

1. Measurements of rate of settling and viscosity as functions of the *pH*.

The colloidal properties of a Wyoming bentonite were examined as a function of the acidity or alkalinity of its water dispersion. The *pH* was measured by means of the hydrogen electrode and calomel cell with alkaline dispersions and a quinhydrone electrode and calomel cell with acid dispersions. By measuring the *pH* of the dispersion and the aqueous phase separated from it by centrifuging, it was found that they were identical, thus proving that equilibrium was attained in this adsorption process.

The stability of the suspension may be measured by the rate of settling of solids when centrifuged at high speed. Suspensions of bentonite containing 5 percent by weight of solids were centrifuged for 5 hours, after which the percent settled and the *pH* were measured. Fig. 1 shows the percentage settled

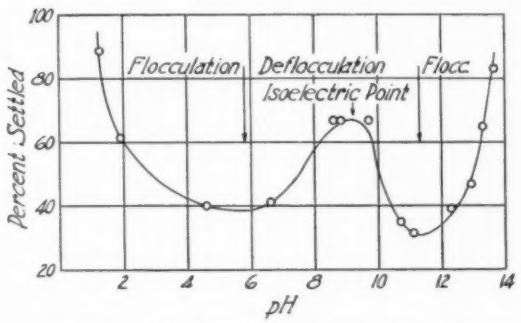

Fig. 1. Percent settled in 5 hours vs. *pH*.

in 5 hours as a function of the *pH*. A colloid is most stable (deflocculated) at the point of minimum rate of settling. The curve shows minimum rates of settling both in acid and in alkaline solutions. The colloid is in its deflocculated condition between $pH = 5.8$ and $pH = 11.4$. At values of *pH* beyond these limits floccuation is attended by increased rates of settling.

The fact that a bentonite swells in water indicates the presence of a certain percentage of colloids of the emulsoid type, stabilized by adsorption of salts contained in the mineral. A certain percentage of the colloids are of the suspensoid type, and these are in excess. Fig. 1 refers to the behavior of the emulsoid content of the suspension. Rate of settling in the deflocculated region is at a maximum at the isoelectric point, of course, for stability depends upon the charge on the particles and the viscosity. As the *pH* increases from the isoelectric point, the hydroxyl ion is increasingly adsorbed, with the rate of settling reaching a minimum value at the limit of deflocculation on the alkaline side, which is also the point of maximum adsorption of the hydroxyl ion. In more strongly alkaline solutions the cation begins a discharging effect on the negatively-charged emulsoid and flocculation begins, with increase in the rate of settling. Similar relations hold on the acid side of the isoelectric

point. In such a colloidal suspension rates of settling are little dependent upon Stokes' law governing the rate of fall of particles in a liquid, for the lower limit of particle size to which this law applies is dependent not only upon viscosities of the fluids but more upon the state of dispersion of the particles.

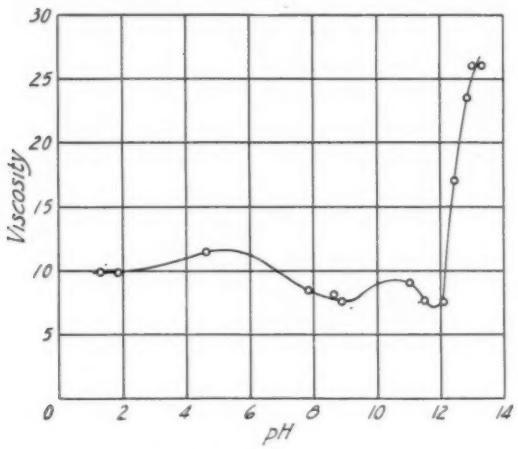

Fig. 2. Viscosity vs. *pH*.

It is evident from a comparison with Fig. 2 that the viscosities measured dynamically are not sufficient to account for the large changes in rates of settling as the *pH* is varied, although there is a close relation between the two curves.

In Fig. 2 it is seen that a minimum viscosity occurs at approximately the *p*H of maximum stabilization as shown in Fig. 1 at $pH = 11.4$. This is to

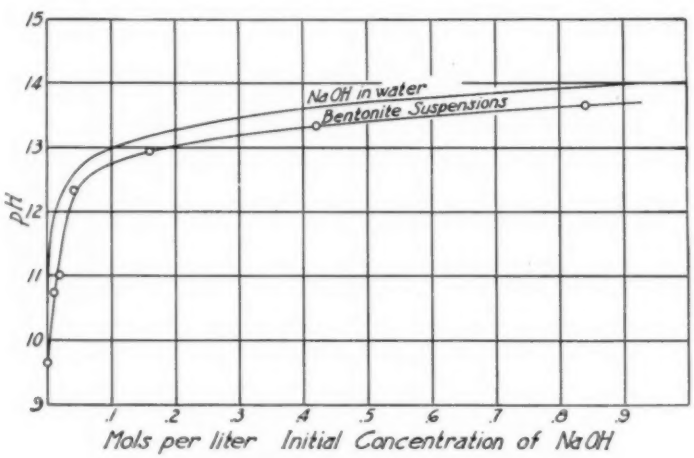

Fig. 3. *pH* of bentonite suspensions vs. alkali added.

be expected, for the electro-viscous effect is necessarily a minimum at this point. On the addition of acid or alkali, attended by adsorption and increase of positive or negative charge, respectively, an increased viscosity is ex-

pected in accordance with Smoluchowski's[5] modified Einstein equation for the effect of electric charges of particles on the viscosity of the fluid. This equation for the electro-viscous effect has been experimentally verified by Kruyt.[6] As the maximum charge is dissipated on further increase in the *pH*, the viscosity must again decrease, reaching a minimum and rising again very rapidly when the colloid is flocculated with gel formation, as shown by the curve on the alkaline side.

The action of alkali upon the bentonite is evidently adsorption. The measured *pH* is not a measure of the alkali added, for alkali disappears from solution. This adsorption of alkali by bentonite is shown in Fig. 3, where *pH* is plotted against added alkali in terms of amount of caustic soda in mols per liter, giving a typical adsorption isotherm.

The viscosity curves of the suspensions indicate that no absolute measure of viscosity can be made of a gelling colloidal suspension. Fig. 4 shows the measured viscosities of two bentonite suspensions with varying speeds of the

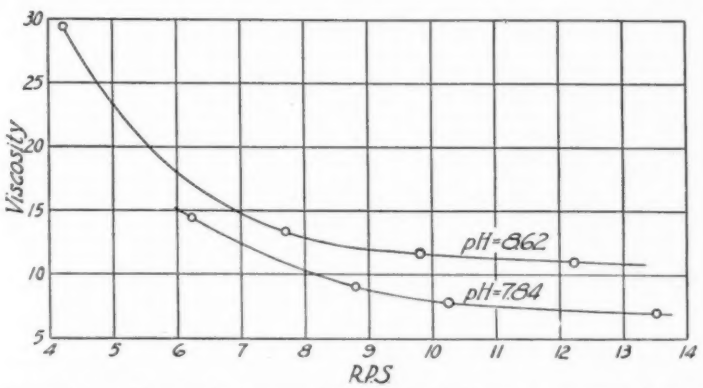

Fig. 4. Viscosities of bentonite suspensions vs. revolutions per second of viscometer.

Stormer viscosimeter; the viscosity is represented as a function of the revolutions per sec. of the cylinder. The viscosity of each suspension is noted to increase sharply with decreased speed of the rotating cylinder, i.e. viscosity decreases with increased shear, a general behavior of hydrophilic sols.[7] This appears to indicate that physical forces in the gel oppose the motion of the particles in other than viscous flow. The viscosities recorded in Fig. 2 were measured at a constant speed of the viscosimeter drum of 10 revolutions per second as a standard.

2. Measurements of swelling.

The swelling of bentonite was measured in alkaline solutions to find the *pH* at which maximum swelling would occur. One gram samples of bentonite placed in uniform tubes were treated with solutions varying in concentration

[5] Smoluchowski, Kolloid-Z. **18,** 194 (1916).

[6] Kruyt, ibid. **31,** 338 (1922).

[7] Hess, Kolloid-Z., **27,** 154 (1920); Hatschek, ibid. **13,** 88 (1913); **7,** 301 (1910); **8,** 34 (1911); **11,** 280, 284 (1912); **12,** 238 (1913).

of caustic soda. These were allowed to stand for 48 hours with occasional agitation to allow contact between various portions of the liquid and solid. The measured volume of the bentonite at the end of this period is plotted against the *pH* of the aqueous phase in Fig. 5. Maximum swelling occurred at $pH = 12.7$, approximately the point of maximum viscosity as shown in Fig. 2. Flocculation is first attended by swelling and then the swelling increases with increased alkalinity. A similar maximum is found in the acid range, but difficulty was experienced in obtaining the equilibrium *pH*. Measurements were not continued in the acid range, for we are interested only in the alkaline range insofar as drilling fluids are concerned.

While it is perfectly possible to control the viscosities and gelling of bentonite gels by the addition of alkali or lime to the suspension, it is desirable from a practical standpoint to treat the solid material in such a way that

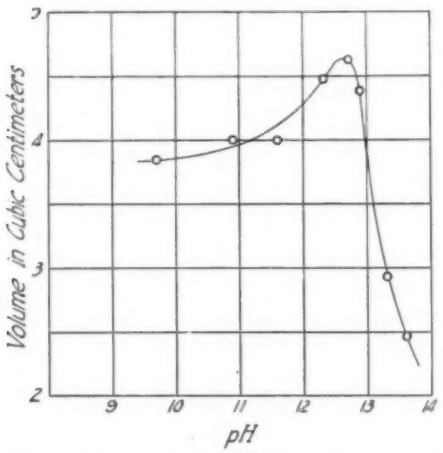

Fig. 5. Volumes occupied by one gram of bentonite vs. *pH*.

rapid gelling takes place on dispersion in water with a minimum amount of material and without further adjustment of the *pH* of the suspension. Most bentonites will form a rigid gel in a 10 percent dispersion in water without further adjustment of the *pH*, but a 4–5 percent dispersion will give the same results when properly treated. It is interesting to note that we were unable to obtain a gel by adding solid caustic soda to the dry bentonite with subsequent dispersion of the mixture, although the *pH* of the resulting dispersion was about 12.7. However, addition of 0.5–1 percent magnesium carbonate to the dry bentonite will result in a rigid gel in a 5 percent dispersion. No doubt the unique properties of magnesium silicates play a role in this case, as well as the proper adjustment of the *pH*.

V. Effect of Salts on the Swelling of Bentonite

The effect of salts on bentonite gels has been studied by Davis and Vacher.[8] Such salts as sodium and potassium chlorides show a marked effect

[8] Davis and Bacher, reference 1.

in prevention of the swelling of bentonites. This effect is particularly desirable in the prevention of trouble due to swelling in drilling through bentonite formations and materials resembling them. Since bentonites from which the salts have been removed by dialysis exhibit neither swelling nor osmotic pressure, it appears that swelling and water absorption are governed by the soluble salts associated with the solid material. The use of salts in the external phase will naturally decrease the activity of water to be adsorbed on the solid surfaces of the mineral crystals, with attendant swelling.

VI. Use of Bentonite in Weighted Drilling Fluids

One of the most useful properties of bentonite in connection with drilling fluids is the stabilization of so-called weighted fluids, suspensions of materials

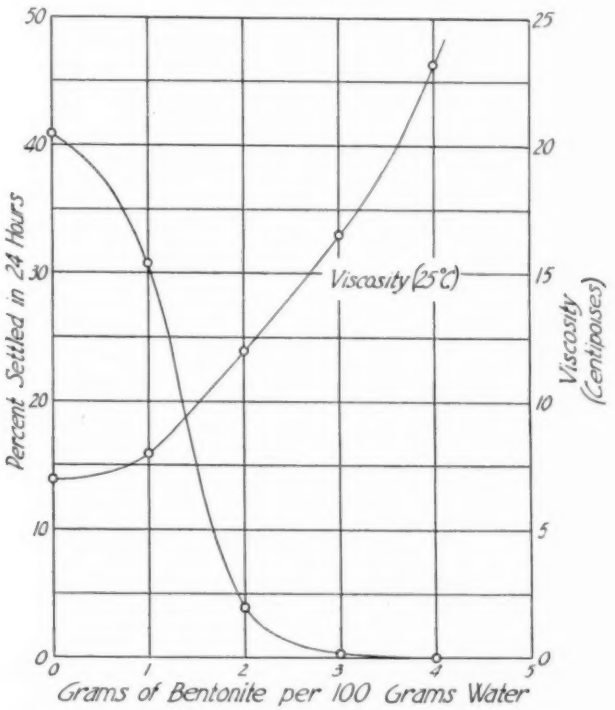

Fig. 6. Amorphous silica suspensions. Density = 1.44.

such as barite, hematite, amorphous silica, etc. These fluids are used for drilling through high pressure gas formations, in order to furnish sufficient hydrostatic pressure to counterbalance the formation pressure. The great difficulty with these suspensions is their tendency to settle in the drill hole, making further progress in drilling impossible in may cases. The addition of relatively small quantities of bentonite to these suspensions has a remarkable stabilizing influence, as shown in Fig. 6 for an amorphous silica suspension of density 1.44; 3 to 4 percent of bentonite (of total water in the suspension) decreases the rate of settling of the suspension from approximately 40 percent in 24 hours

to practically zero in the same time. The viscosity curve of the suspension rises rapidly on the addition of bentonite, as shown in Fig. 6.

The explanation of this large decrease in rate of settling is furnished by the data plotted in Fig. 7, where the deflection in arbitrary units of the suspended cylinder of a MacMichael viscosimeter is plotted against the time in minutes, i.e. the relaxation curve.[9] A residual deformation is maintained permanently due to gel formation of the added bentonite. As seen from the curves of Fig. 7 an amorphous suspension of density 1.44 has zero residual deformation, while the addition of sufficient bentonite to stabilize the suspension results in a definite value for residual deformation. A heavier suspension

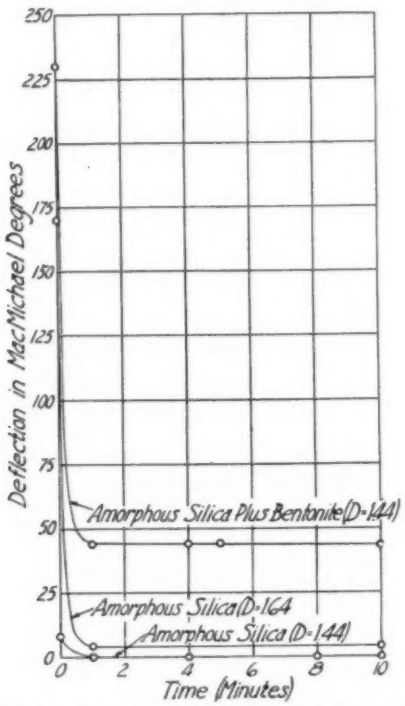

Fig. 7. Residual torque of amorphous silica suspensions.

(density 1.64) prepared from amorphous silica alone to have the same viscosity as the lighter suspension plus bentonite had a very small residual deformation value, as shown in Fig. 7.

Gel formation, with attendent arrest of settling of suspensions, by addition of bentonite,[10] or chemicals in the case of clay suspensions, is finding increased application in the art of drilling oil wells.

[9] See Schwedoff, J. Physique (2) **8**, 341 (1899); Hatschek and Jane, Kolloid-Z. **39**, 300 (1926).

[10] Several varieties of treated bentonite are sold for this purpose under various tradenames, such as "Aquagel."

THE EDITOR'S COLUMN

IF THE ability to get others to do his work is a mark of anything, your Editor can qualify. This month Professors Buchta and Hill of the University of Minnesota comment in these columns on various topics which have been the subject of articles in recent issues of the Physical Review.

The hot summer months are not altogether happy ones for initiating anything. I am sorry that it will be necessary again to defer the appearance of the section "Engineering News and notes."

J. T. T.

X-ray Wave-lengths, Crystal Structures and Fundamental Constants

IN ADDITION to discovering new phenomena and facts, physicists are attempting to describe more accurately those previously observed in nature. These descriptions are always eventually given in numerical terms and the refinements in description involve increased precision in measurements. In the past such increased precision has sometimes led to the discovery of new phenomena and also allowed more critical tests to be made of theories relating different phenomena. The measurement of x-ray wave-lengths is one which can now be made by several methods and with high precision. The disagreement in the results obtained by using the different methods requires that the values of some of the fundamental constants be changed from their previously accepted values or that some new characteristics of crystal structures be taken into consideration.

Some few years ago it was found possible to secure x-ray spectra from ruled reflection gratings if the glancing angle was very small. In the experimental arrangement the beam of x-rays strikes the surface at an angle usually smaller than one degree. At these small angles the K lines from the heavier elements Cr, Cu, Mo, etc., undergo total internal reflection. A narrow beam of x-rays upon striking the ruled grating then yields two or more beams, the reflected beam and one or more diffracted beams. The angles to be measured are very small but by recording the reflected and diffracted beams on two photographic plates spaced a known distance apart and making arrangements to record the direct beam on the same plates, the measurement of the angles is reduced to linear measurements of the spacing of lines on the plates and the distance between the plates.

In a paper published in the May 15 issue of the PHYSICAL REVIEW by J. A. Bearden, the results of a long and carefully performed series of measurements of the wave-lengths of the Cu and Cr K x-rays are given. The method used was that described above. Possible errors in the grating, those due to divergence of the beam, the shrinking of the emulsion on the plate, etc. were either eliminated or their value determined. The results obtained are given in the third column of the following table of wave-lengths.

The wave-lengths as determined by Mr. Bearden depend entirely on length measurements described above and the constant of the ruled grating, also a linear measurement. The wave-lengths are calculated from the usual grating formula

$$n\lambda = d(\sin i - \sin r)$$

or its modification for small angles. In these equations n is the order of the spectral line, d distance between rulings on the grating and i and r the angles of incidence and diffraction respectively. There seems to be no reason for

TABLE I

Spectral Line	Crystal λ	Grating λ	Limiting Error	Grating λ − Crystal λ
Cu $K\alpha$	1.38914A	1.39225A	±0.00014	+0.224%
Cu $K\alpha$	1.53838	1.54172	±0.00015	+0.217
Cr $K\beta$	2.08017	2.08478	±0.00021	+0.222
Cr $K\beta$	2.28590	2.29097	±0.00023	+0.222

questioning the methods of the measurements or the use of the measurements in calculating the wave-lengths. The wave-lengths so obtained, however, differ from the previously accepted values obtained by using crystals by an amount very much larger than the known probable errors of either group of measurements. The differences in percent are given in Table I above. The wave-lengths obtained by using crystals are consistently shorter than those obtained by the use of gratings.

These differences are in themselves interesting but are particularly so because of the entangling alliances of the crystal wave-lengths. The crystal wave-length is determined by the Bragg law of diffraction,

$$n\lambda = 2d \sin\theta\left(1 - \frac{1-\mu}{\sin^2\theta}\right) \qquad (1)$$

in which μ is the index of refraction of the x-rays in the crystal, θ the angle of diffraction, and d the grating space of the crystal. The grating space of the crystal is calculated in terms of Avogadro's number and the crystal form. Thus for a simple cubic crystal we have

$$d = (M/N\rho)^{1/3} \qquad (2)$$

in which N is the number of molecules per mole, M the molecular weight and ρ the density of the crystal. Using the value of λ from ruled grating measurements and putting it in equation (1) above we may obtain a value for d which when substituted in equation (2) gives a value for N, Avogadro's number. When this is done, using constants from Birge's tables, one finds

$$N = 6.019 \times 10^{23} \text{ mol. per mole}$$

as compared to

$$6.064 \times 10^{23}, \text{ the accepted value.}$$

Using this value of N and the Faraday constant F, we find the charge on the electron e as

$$e = F/N = 4.806 \times 10^{-10} \text{ e.s.u.}$$

The value given by Millikan is 4.770×10^{-10} e.s.u.

From this value of e we may obtain a corresponding value of h, Planck's constant, by using the quantum relation

$$Ve = h\nu = hc/\lambda = hc/2d \sin\theta\left(1 - \frac{1-\mu}{\sin^2\theta}\right)$$

in which V is the potential applied to the x-ray tube, c the velocity of light and λ the minimum wave-length of the continuous x-ray spectrum. Using the results given by Duane, Palmer and Yeh for the applied potential V and the angle of diffraction we may find the value of h. If in this calculation we use the ruled grating wave-length but take $e = 4.770 \times 10^{-10}$ e.s.u. we obtain

$$h = 6.573 \times 10^{-27} \text{ erg sec}$$

as compared to 6.547×10^{-27} as given by Birge. If we use the ruled grating wave-length and the value of e as 4.806×10^{-10} e.s.u. we obtain $h = 6.623 \times 10^{-27}$ erg sec.

In the first value of h given above we assumed the accepted value of e rather than the value given by grating wave-length measurements. But even this value of h differs from the accepted value by an amount much larger than the probable experimental error.

The values of N, e and the last value of h as calculated from the ruled grating wave-lengths assume a perfect crystal lattice. It seems at present that the only possible way of accounting for the discrepencies is to assume some imperfections or variations in the crystal lattice. The constants N, h and e determine modern physical calculation through so many interlocking directorates that it is difficult to accept the high values given by these x-ray measurements. Recently Zwicky and others have considered variations in the crystal lattice of crystals to account for their various physical properties. In particular, it is assumed that there is a concentration of atoms at rather regularly spaced intervals, giving a mosaic structure to the crystal and thus making the average density higher than the density of the parts of the crystal effective in diffracting x-rays. Such a variation would yield crystal wave-lengths that were too short, when the calculations assumed a perfect crystal. The presence of fine cracks in the crystal, which may be present in some cases, would offer no explanation as the correction necessary has the wrong sign.

In conclusion then it seems proper to accept Mr. Bearden's values for the x-ray wave-lengths as correct and to assume that the differences of his measurements from the crystal wave-lengths are due to crystal imperfections. In fact the results may be considered as evidence for the mosaic structure of crystals. If the grating wave-lengths here are correct, the true grating space of a calcite crystal is

$$d = 3.0359 \text{ Anstrom units.}$$

As this value is 0.22 to 0.25 percent higher than values previously used, all wave-lengths

based on calcite crystal measurements would therefore need to be increased by that fraction.

J. A. Bearden, "Absolute Wave-Lengths of the Copper and Chromium *K*-Series," Phys. Rev. **37,** 1210 (1931).

R. T. Birge, "Probable Values of the General Physical Constants," Phys. Rev. Supp. **1,** 1 (1929).

R. A. Millikan. "The Most Probable 1930 Values of the Electron and Related Constants," Phys. Rev. **35,** 1231 (1930).

F. Zwicky, "Zur Mosaikstrukturen der Kristalle," Helvetica Physica Acta **3,** 269 (1930).

—— "Possible Influence of Mosaic Structure of Crystals on the Determination of Avogadro's Number," Proc. Nat. Acad. Sci. **16,** 211 (1930).

—— "Mosaic Crystals," Proc. Nat. Acad. Sci. **15,** 816 (1929).

W. Duane, H. H. Palmer and C. Yeh, "A Remeasurement of the Radiation Constant, *h*, by Means of X-Rays," Jour. Opt. Soc. Am. **5,** 376 (1921).

J. W. BUCHTA

Hyperfine Structure and the Constitution of Nuclei

THE unravelling of the problem of the structure of the nuclei of the various atoms is one of the most weighty questions facing physicists today. We now believe that there are but two primary elements out of which all matter is constructed; i.e. the electron and the proton, the latter being the nucleus of the simplest of the atoms, hydrogen. The nuclei of all of the other atoms are supposed to be made up of electrons and protons. From the well-known relations between the atomic weights and the atomic numbers of the elements as expressed in Mendeleeff's periodic table, one can estimate the number of protons and the number of electrons in each of the atomic nuclei, but we cannot as yet tell just what the dynamical constitution of these systems may be.

Within the last five or six years, however, advances have been made in both theory and experiment which give promise of ultimate success. One of the most interesting of these advances has been the interpretation of the hyperfine structure of the spectral lines due to the atoms. It is well known that under relatively low dispersion it is quite usually the case that the spectral lines of an atom are grouped together in sets of a few lines, as for example the ordinary yellow doublet of Na at 5890 and 5896A respectively. This grouping of the lines is called a "fine structure" or "multiplet structure," and is quite well accounted for by the new quantum mechanics of the atom in terms of the structure of the electron shells alone. So far as the explanation of this feature of the spectrum is concerned, the nucleus might just as well be a single point charge with charge *Ze*. If, however, the spectrum is examined with instruments of very high resolving power it is found that in many, although by no means in all, cases the lines of the fine structure pattern which before seemed single, actually have a complex structure, being themselves composed of a series of very closely spaced lines. This finer arrangement of lines is referred to as a "hyperfine structure," and it is in the explanation of the origin of this structure that new light is shed on the properties of the nuclei.

It was suggested in 1927 by W. Pauli, Jr. in Germany, that this hyperfine structure might be attributed to the presence of an intrinsic vector angular momentum and a corresponding magnetic moment associated with the nucleus.[1] This means that the nucleus can no longer be treated as a point charge, but account must be taken of its complex structure. As the electrons fly about in their peregrinations within the atom they are disturbed slightly by the presence of this tiny magnetic moment. According to the theory the principal result of this interaction is that the energy levels which the atom would have if the nucleus were simply a point charge, are actually split up into a number of separate components which, however, lie very close together, since the electrons are disturbed but very little by the magnetic moment of the nucleus. As the lines of the spectrum arise from transitions between the energy levels of the atom, this structure of the energy levels is mirrored in the structure of the spectrum, giving rise to the hyperfine structure which is observed.

[1] Cf. R. de L. Kronig and S. Frisch, Phys. Zeits. **32,** 457 (1931), for a summary of the present status of the problem of nuclear moments for a more general standpoint than was possible here.

The way in which the lines of the hyperfine structure patterns are grouped; i.e. the number and separations of the components of which each line of the ordinary multiplets are composed, depends according to the theory upon the kind of motion which the electrons perform within the atom. For electron orbits of the so-called penetrating s type in which the electron is quite near the nucleus for a good share of the time, the disturbing effects of the nuclear moment are largest and the theory is in best agreement with the experimental results. It was just these cases, of course, which were normally found and studied first.

Within the last few months cases in which the valence electrons are not in s orbits have been examined, and here difficulties have been found in the theory. This is emphasized particularly in recent papers of Goudsmit[2] and Breit.[3] The former examines particularly the behavior of the separations of the hyperfine structure components for various kinds of coupling among the valence electrons, which are assumed not to be in s states. It is found that the theoretical formulae do not fit the experimental data very well particularly for Bi and Tl, and the conclusion to which Goudsmit comes is that the expression which is used for the calculation of the interaction of the electron spin with the nuclear spin is somehow incorrect and so is to blame for the discrepancies.

Breit re-investigates the whole problem anew for the particular case of a single valence electron in a p state; an electron configuration which gives rise to an ordinary doublet term of the type $p_{\frac{1}{2}}$ and $p_{1\frac{1}{2}}$, each term of which is in turn to show a hyperfine structure. Whereas Goudsmit used a non-relativistic method, Breit bases his calculation on the relativistic wave equation of Dirac, finding it necessary to use some approximations in order to get numerical results since the exact equation cannot be readily solved for this problem. The final result is a value for the ratio of the separation of components of the hyperfine structure in the $p_{\frac{1}{2}}$ term to the separation in the $p_{1\frac{1}{2}}$ term. On comparison with the measurements of Wulff on Tl I this ratio proves to be too small by a factor 2, while the non-relativistic theory gives a ratio too small by a factor 3.4. Thus the new computation improves the result, but shows that the theory is still in need of improvement.

The work on hyperfine structure gains much of its importance from its relation to the properties of nuclei. Quite apart from the question of the dynamics of the interaction of the nucleus and the outer electrons in the atom, which is the subject of the papers discussed above, the measurement of hyperfine patterns is important because it leads to a determination of the numerical magnitudes of the angular momenta of the various nuclei. This is of prime importance in the study of isotopes, radioactive atoms, and in numerous fields. It is fairly certain now that both the proton (hydrogen atom nucleus) and the electron have themselves intrinsic angular momenta of amount $\frac{1}{2}$, measured in Bohr units $h/2\pi$ the so-called "spins." According to the theory for the vector composition of the angular momenta of electrons and protons in the building up of nuclei, it ought to be the case that the resultant "spin" angular momentum of a nucleus composed of P protons and E electrons should be an integer $(0, 1, 2, \cdots)$ if $(P+E)$ is even, and should be a half-integer $(\frac{1}{2}, 1\frac{1}{2}, \cdots)$ if $(P+E)$ is odd. All angular momenta are measured in units $h/2\pi$, of course. Here too there seems to be a lack of agreement between present theory and experiment, since for the nitrogen nucleus $P+E(=14+7=21)$ is odd, whereas experiment indicates that the N nucleus has an integral valued resultant angular momentum, probably 1. This particular fact was determined not from hyperfine structure measurements, but from Raman effect[4] and band spectra.[5] It has been suggested by Heitler and Herzberg that maybe the electron loses its spin when in the nucleus, and according to Langer this may come out as a result of the new interpretation which has been put on quantum mechanics by Schrödinger.[6]

E. L. Hill

[2] S. Goudsmit, Phys. Rev. **37,** 663 (1931).

[3] G. Breit, Phys. Rev. **38,** 463 (1931).

[4] F. Rasetti, Proc. Nat. Acad. Sci. **15,** 515 (1929).

[5] R. S. Mulliken, Trans. Faraday Soc. **25,** 634 (1929).

[6] W. Heitler and G. Herzberg, Naturwiss. **17,** 673 (1929). R. M. Langer, Phys. Rev. Aug. 15, 1931. E. Schrödinger, Sitz. Ber. d. Preuss. Akad. **3,** 63 (1931).

Theories of the Electron

EVER since the latter part of the nineteenth century when the electron theory began to play a prominent rôle in physics, mathematical physicists have been trying to find a satisfactory model for the electron itself. The calculation of the mass of the electron from the properties of its electromagnetic field was a high point in the classical theory, but was soon quite over-shadowed by Einstein's proposal of the relativistic expression for the variation of inertial mass with velocity. For most purposes the electron has been treated simply as a charged mass point.

When Uhlenbeck and Goudsmit[7] discovered in 1925 that it is very convenient in the interpretation of the spectra of atoms to assume that the electron has a mechanical angular momentum ("spin") of amount $\frac{1}{2}$ (units $h/2\pi$), the whole question of the constitution of the electron was re-opened. Since that time the conception of electron spin has proved its usefulness in many branches of atomic physics. Frenkel and Thomas,[8] using the idea of an electron actually in rotation about an axis of symmetry, did succeed in calculating the correct value for the ratio of the mechanical angular momentum to the magnetic moment of the electron. Neither of these investigators used the ideas of the new quantum mechanics since these were just being developed at that time. Due to the now historic work of Dirac,[9] the theory of the spin has actually been incorporated as an integral part of quantum mechanics. Dirac's wave equation for the electron has attracted great attention since it satisfies the requirements of the special theory of relativity and also predicts the existence of the spin. Spin and relativity have thus become associated in a very intimate way.

When this equation was studied in detail it was discovered that it embodies some predictions of a very startling sort. Chief among these is the prediction that when exposed to the influence of electromagnetic radiation, the electron ought to act just as though it were capable of changing the sign of its charge, and so of becoming a particle of charge $+e$, a "positive" electron.[10] This was very startling, but Dirac[11] again came to the rescue with the idea that perhaps the universe is full of electrons of this new type, and that when one of them changes sign and so becomes an ordinary electron, the "hole" which is left in the infinite density of "positive" electrons is to be interpreted as being a kind of proton. In many ways this is an intriguing theory, but it has the obvious difficulty that the mass associated with such a "hole" is equal to the mass of the electron and not to the mass actually observed for the proton.

Quite recently Schrödinger[6] has made a suggestion which promises to do away with this difficulty. This is discussed in a recent paper of Langer.[12] The suggestion is of a mathematical rather than of a physical nature, having to do with the restriction of the kind of operator allowable in the quantum mechanics in such a way that the unpleasant transitions of the type discussed above have zero probability of occurrence.[13] As an alternative suggestion, Langer proposes to modify the expression for the mutual interaction of two particles in such a way that the same result is obtained. These theories have not been studied in sufficient detail as yet to give a real indication of their generality, but they do seem to offer possible avenues for escape from the difficulties of the earlier work, and are indicative of new methods of approach to the problem.

E. L. HILL

[7] G. Uhlenbeck and S. Goudsmit, Nature **117,** 264 (1926).

[8] J. Frenkel, Zeits. f. Physik **37,** 243 (1926). L. Thomas, Phil. Mag. **3,** 1 (1927); Nature **117,** 514 (1926).

[9] P. A. M. Dirac, Proc. Roy. Soc. **A117,** 610 (1928).

[10] Cf. e.g. O. Klein, Zeits. f. Physik **53,** 157 (1929). J. R. Oppenheimer, Phys. Rev. **35,** 461 (1930).

[11] P. A. M. Dirac, Proc. Roy. Soc. **A126,** 360 (1930).

[12] Schrödinger's paper is not available at present to the writer, and is known to him only through the discussion of Langer.

[13] It is not clear from Langer's paper what the connection is between Schrödinger's even and odd functions and the symmetry properties of the wave equation. It is implied that the separation of operators and functions into two classes is of a purely arbitrary nature.